Metabolic Engineering 70 (2022) 89–101

Contents lists available at ScienceDirect

Metabolic Engineering

journal homepage: www.elsevier.com/locate/meteng

Overexpression of OsMYBR22/OsRVE1 transcription factor simultaneously enhances chloroplast-dependent metabolites in rice grains

Ye Sol Jeong [a,b,1], Heebak Choi [a,1], Jae Kwang Kim [c], Seung-A Baek [c], Min-Kyoung You [a], Dongho Lee [b], Sun-Hyung Lim [d,**], Sun-Hwa Ha [a,*]

[a] Department of Genetics and Biotechnology, College of Life Sciences, Kyung Hee University, Yongin, 17104, Republic of Korea
[b] Department of Biotechnology, College of Life Sciences and Biotechnology, Korea University, Seoul, 02841, Republic of Korea
[c] Division of Life Sciences and Bio-Resource and Environmental Center, Incheon National University, Incheon, 22012, Republic of Korea
[d] School of Biotechnology, Division of Horticultural Biotechnology, Hankyong National University, Anseong, 17579, Republic of Korea

ARTICLE INFO

Keywords:
Carotenoids
Chlorophylls
Chloroplasts
Essential amino acids
GABA
MYB-Related TF

ABSTRACT

The *OsMYBR22* (same to *OsRVE1*), an R1type-MYB transcription factor belonging to the rice CCA1-like family, was upregulated under blue light condition, which enhanced the chlorophyll and carotenoid accumulation. The overexpression of *OsMYBR22* in rice (*Oryza sativa*, L) led to everlasting green seeds and leaves of a darker green. Transgene expression patterns showed more concordance with chlorophyll than carotenoid profiles. The transcript levels of most genes related to chlorophyll biosynthesis and degradation examined were similarly repressed in the late maturing stages of seeds. It proposed that rice seeds have the feedback regulatory mechanism for chlorophyll biosynthesis and also implied that evergreen seed traits might be caused due to the inhibition of degradation rather than the promotion of biosynthesis for chlorophylls. Metabolomics revealed that *OsMYBR22* overexpression largely and simultaneously enhanced the contents of nutritional and functional metabolites such as chlorophylls, carotenoids, amino acids including lysine and threonine, and amino acid derivatives including γ-aminobutyric acid, which are mostly biosynthesized in chloroplasts. Transmission electron microscopy anatomically demonstrated greener phenotypes with an increase in the number and thickness of chloroplasts in leaves and the structurally retentive chloroplasts in tubular and cross cells of the seed inner pericarp region. In conclusion, the molecular actions of *OsMYBR22/OsRVE1* provided a new strategy for the biofortified rice variety, an "Evergreen Rice," with high accumulation of chloroplast-localized metabolites in rice grains.

1. Introduction

The autotrophic life of plants depends on chloroplasts, the site of photosynthesis (Waters and Langdale, 2009; Choi et al., 2021). Other metabolic pathways essential for plant survival occur in chloroplasts, which contain biological reactions for carbohydrates, amino acids, lipids, and photosynthetic pigments such as chlorophylls and carotenoids (Chen et al., 2018). Light is the most important factor in the stimulation of pigment biosynthesis and chloroplast development (Llorente et al., 2017; Yuan et al., 2017). The physiologically close relationship between chloroplast biogenesis and metabolisms of chlorophylls and carotenoids has often been reported in pleiotropic phenotypes according to diverse light condition. Particularly, blue light promoted photosynthesis, triggered chloroplast development, and enhanced the accumulation of photosynthetic pigments, resulting in phenotypic changes that include darker green color and shorter height due to the inhibited stem elongation, wider breadth, and larger leaf angle (Christie, 2007; De Wit et al., 2016; Ouzounis et al., 2015). Increased pigment content such as chlorophylls, carotenoids, and phenolic compounds by blue light irradiation has been intensively reported in various horticultural plant species, including *Cymbidium* (Tanaka et al., 1998), lettuce (Li and Kubota, 2009), red lettuce (Johkan et al., 2010), broccoli (Kopsell and Sams, 2013), and *Kalanchoe pinnata* (Nascimento et al., 2013). These increases in pigment contents serve to enhance the functional and nutritional value of the plant materials. The levels of other metabolites such as amino acids, organic acids, fatty acids, and

* Corresponding author.
** Corresponding author.
E-mail addresses: limsh2@hknu.ac.kr (S.-H. Lim), sunhwa@khu.ac.kr (S.-H. Ha).
[1] These authors contributed equally to this work.

https://doi.org/10.1016/j.ymben.2021.12.014
Received 30 August 2021; Received in revised form 25 December 2021; Accepted 30 December 2021
Available online 13 January 2022

flavonoid glycosides were relatively high in blue light-treated rice leaves with the enhanced antioxidant activities (Jung et al., 2013).

When the plants are exposed to light that includes blue light, receptor proteins such as cryptochromes, phototropins, phytochromes, and UV RESISTANCE LOCUS 8 carry out photoreception. Post-translational regulation by inhibiting E3 ligase-mediated degradation pathways of light signal proteins cooperatively works with transcriptional regulation by transcription factors (TFs) for photomorphogenesis including photosynthesis, chloroplast development, and chlorophyll and carotenoid biosynthesis (Lau and Deng, 2012; Martín et al., 2016; Tang et al., 2016; Paik and Huq, 2019; Choi et al., 2021). TFs have been reported as core positive regulators. LONG HYPOCOTYL5 (HY5) controls light-responsive gene transcription by direct interaction with ACGT element-containing motifs including G-boxes (CACGTG) in the promoters of genes such as *light-harvesting complex* (*Lhc*) *b* and *phytoene synthase* (*PSY*) (Andronis et al., 2008; Toledo-Ortiz et al., 2014). Its binding activity was increased after physical interaction as HY5-CIRCADIAN CLOCK-ASSOCIATED1 (CCA1) for *Lhcb*, and it formed an antagonistic regulatory module as HY5-PHYTOCHROME -INTERACTING FACTOR (PIF) for *PSY* in *Arabidopsis*. CCA1 directly affected activation of *GOLDEN2-LIKE* (*GLK*) *2* and suppressed *ORESARA1* (*ORE1*), which counteracts the GLK function in *Arabidopsis* (Song et al., 2018). GLK1 and GLK2 have been studied as key regulators at the center of a light-induced transcriptional network to govern photomorphogenesis overall in maize, rice, *Arabidopsis*, and tomato (Rossini et al., 2001; Nakamura et al., 2009; Waters et al., 2009). Also, rice PIF-like (PIL) 1, the closest homolog of *Arabidopsis* PIF4, promoted chlorophyll biosynthesis through a feed-forward loop: PIL1 upregulates *GLKs* and two chlorophyll biosynthetic genes such as *protochlorophyllide oxidoreductase* (*POR*) *B* and *chlorophyllide a oxygenase* (*CAO*) *1*; GLKs then activate *PORB*, *CAO1*, and two photosynthetic apparatus genes, *Lhca* and *Lhcb* (Sakuraba et al., 2017).

Previously, we have reported the highest amounts of carotenoids and phenolic compounds with darker and shorter phenotypes of rice plants under blue light-emitting diode illumination. Our studies suggest 11 candidate genes including two myeloblastosis (MYB)-related TFs, the rice *RADIALIS-LIKE3* (*OsRL3*), and *OsMYBR22*, which were upregulated in blue light versus white light (Lakshmanan et al., 2015). Our results proposed the possibility that these TFs function as blue light-mediated transcriptional modules to promote plant greening phenotypes. While OsRL3 has been shown to function as a positive regulator of leaf senescence (Park et al., 2018), the biological roles of OsMYBR22 (designated as a serial number among the *Grasses* MYB-related TFs) have been studied very little (Gray et al., 2009; Smita et al., 2015): a CMYB1 with the only cold-inducible gene expression property (Duan et al., 2014) and a rice CCA1-like REVEILLE (OsRVE) 1 with just amino acid sequence homology (Linde et al., 2017).

The MYB family of TF proteins is large and functionally diverse being represented in all eukaryotes including plants (Ambawat et al., 2013). They are classified into four subfamilies, MYB-related/1R-MYBs/R1type-MYBs, 2R-MYBs/R2R3-MYBs, 3R-MYBs/R1R2R3-MYBs, and 4R-MYBs, according to the number and position of an MYB DNA-binding domain repeat, which is a helix-turn-helix structure of 51–53 amino acids. Their regulatory functions are involved in cell differentiation, development, secondary metabolism, responses to biotic and abiotic stresses, and light and phytohormone signaling pathways (Chen et al., 2006; Dubos et al., 2010; Ambawat et al., 2013). At least 197 and 155 MYB TFs were predicted in the *Arabidopsis* and rice genomes, respectively (Chen et al., 2006; Katiyar et al., 2012). Particularly, in terms of light regulation, the central circadian oscillators CCA1 and LATE ELONGATED HYPOCOTYL (LHY) are encoded by two *Arabidopsis* genes (*AtCCA1* and *AtLHY*) and a rice gene (*OsCCA1/OsLHY*) belonging to the MYB-related subfamily (Lu et al., 2009; Nagel et al., 2015; Shen et al., 2015).

Our interest for this study in that the TF, an OsMYBR22, was predicted as one of the OsCCA1-like proteins in rice. We constitutively overexpressed an *OsMYBR22* and observed typical blue light-treated phenotypes involving reduced height and greener leaf color of rice plants. Moreover, it resulted in the prolonged green color of seeds even after ripening. Through physiological, molecular, metabolite-analytical, and microscopy approaches, we confirmed that the ectopic expression of an *OsMYBR22* TF enhanced nutritional and functional qualities of rice grains.

2. Materials and methods

2.1. Rice plant materials and growth conditions

Japonica-type Korean rice (*Oryza sativa* L. cv. Dongjin) was used for gene cloning, analyzing gene expression, preparing protoplasts, and generating transgenic plants. Seeds were sterilized with 70% ethanol and 2% sodium hypochlorite, germinated on Murashige and Skoog media with 1.5% (w/v) sucrose for 5 days in a growth chamber with a 16-h light/8-h dark cycle at 28 °C, transplanted into soil, and then grown in a greenhouse under natural light conditions. Particularly, seeds were germinated and grown on MS media for 7 days under either blue (450 nm) or white (mixture of blue, green (530 nm), and red (660 nm)) light conditions with photosynthetic photon flux density at 95 μmol/m^2/s, 10 days under 9 days dark/1 day light for protoplast isolation, and 7 days under a 16-h light/8-h dark cycle for germination tests in a growth chamber. Transgenic rice plants were regenerated according to shooting and rooting procedures on selection media that included phosphinothricin (3 mg/L) and carbenicillin (250 mg/L) in a growth chamber as previously described, with slight modifications (Hiei et al., 1994), after which they were grown in soil in a greenhouse during all seasons or in a paddy field at Kyung Hee University in Yongin, South Korea (37° 24′ N latitude, 127° 08′ E longitude), during the summer season until maturity. To evaluate the agronomic traits of transgenic plants, T_4 homozygous lines were grown in a paddy field during the summer, and yield parameters were scored for 30 plants per line. When the plants had reached maturity and the grains had ripened, they were harvested and threshed. The unfilled and filled grains were separated, weighed, and independently counted using a Countmate MC1000H (Motex Ltd., Seoul, Korea). The following agronomic traits were scored: panicle length (PL; cm), culm length (CL; cm), filling rate (FR; %), total grain weight (TGW; g), 100-grain weight (100 GW; g), total number of grains (TNG; g), number of panicles per plant (NP), and number of spikelets per panicle (NSP). The data were analyzed using Student's *t*-test in Microsoft Excel, and differences were considered significant at $p < 0.001$ (***), $p < 0.01$ (**), or $p < 0.05$ (*).

2.2. Vector construction and molecular analysis of transgenic plants

The coding sequence of *OsMYBR22* (1476 bp, LOC_Os02g46030) was amplified from seedling cDNAs of rice (*Oryza sativa* L. cv. Dongjin) using primer sets (Supplementary Table S1) based on the information provided by the Rice Full-Length cDNA Consortium (https://www.ncbi.nlm.nih.gov/nuccore/AK111726). Two GFP fusion vectors, *pOsMYBR22:sGFP* and *peGFP:OsMYBR22*, for rice protoplast transfection were prepared through the In-Fusion HD Cloning kit (Clontech, Mountain View, CA) using *pGA* cloning vector series No. 3452 and 3652, respectively, to analyze the subcellular localization (Kim et al., 2009). Rice overexpression vectors of *pOsMYBR22:Myc* and *pMyc:OsMYBR22* were constructed through an In-Fusion Cloning (Clontech) using two *myc*-tagged entry vectors, *pE3c* and *pE3n*, and then Gateway cloning using a destination *p700* vector carrying the 5' upstream region of rice *phosphogluconate dehydrogenase 1* (*PGD1*) gene as a constitutive promoter (Dubin et al., 2008; Park et al., 2010).

After rice transformation, 2-week-old leaf tissues of putative transgenic plants were homogenized by a TissueLyser II (Qiagene, Hilden, Germany) and used for the preparation of total proteins, genomic DNAs, and total RNAs. The proteins were extracted in a buffer (50 mM Tris-HCl

(pH 7.6), 150 mM NaCl, 0.1 mM sodium deoxycholate, 1% Triton X-100, 0.1% SDS, 2 mM EDTA, and 1x complete protease inhibitor cocktail), and their concentrations were measured using a Quant-i™ Protein Assay Kit (Invitrogen, Waltham, MA). Western blotting was performed on each sample, which consisted of 60 μg of total protein, by binding of primary anti-MYC antibodies (1:2000, 9E10, Santa Cruz Biotechnology, CA) followed by anti-mouse IgG (whole molecule) peroxidase-conjugated secondary antibodies (1:100000, A9044, Sigma-Aldrich, St. Louis, MO). The signal bands were developed using a BCIP/NBT color development system (Promega, Madison, WI) and imaged using a UVITEC camera (Cleaver Scientific, Warwickshire, UK). The genomic DNAs from T_0 leaf tissues were prepared using a DNeasy Plant Mini Kit (Qiagen), and TaqMan PCRs were used to detect the *Bar* transgene as previously described (Ko et al., 2018). A value of 1 was calculated for the genomic DNAs of *stPAC 25* rice, with a homozygous single copy of the *Bar* gene used as a positive control (Jeong et al., 2017). RNA-associated methods are comprehensively described below.

2.3. Quantitative real-time RNA analysis

Total RNAs were isolated from leaves and unpolished seeds during the developmental stages of both nontransgenic (NT) and transgenic rice plants. Frozen powder samples of leaves and seeds were extracted using RNeasy Plant Mini Kit (Qiagen) in conjunction with PureLink® Plant RNA Reagent (Invitrogen). The RNAs were treated with DNase I treatment (Qiagen), and their quality and concentration were checked by a NanoDrop ND-2000 Spectrophotometer (Thermo Scientific, Waltham, MA). The cDNAs were simultaneously synthesized and amplified with 1 μg of total RNA using AccuPower® RT Premix (Bioneer, Daejeon, Korea). The following amplification was performed using iQ™ SYBR Green Supermix (Bio-Rad, Hercules, CA) in a CFX connect real-time system (Bio-Rad). Each reaction consisted of 20 ng of cDNA, each gene-specific primer at 0.3 μM, and 10 μL of SYBR green real-time PCR master mix (Bio-Rad) at a total volume of 20 μL. The PCR conditions were as follows: 3 min at 95 °C, followed by 40 cycles of 15 s at 95 °C and 30 s at 60 °C. Quantitative PCRs (qRT-PCRs) were carried out in triplicate or quadruplicate for three individual plants. Data were presented as formula $2^{-\Delta Ct}$ with ±standard deviation after each Ct value was normalized with the rice *ubiquitin 5* (*OsUBQ5*, Os01g22490) as an internal control and analyzed using Student's *t*-test in Microsoft Excel, and significant differences were considered at $p < 0.001$ (***), $p < 0.01$ (**), or $p < 0.05$ (*). All qRT-PCR primer sequences are listed in the supporting information (Supplementary Table S1).

2.4. Quantification of chlorophylls, carotenoids, and phenolic compounds

Rice leaves and seeds were powdered to extract pigment metabolites. Total chlorophylls were extracted using 100% methanol at 70 °C for 30 min with shaking at 500 rpm using a Thermomixer Comport (Eppendorf AG, Hamburg, Germany). The contents of chlorophyll *a and b* were calculated using Wellburn's formula with absorbance of the supernatant that was measured at 666 and 653 nm using a spectrophotometer (Optizen Pop, Mecasys Co., Daejeon, Korea). Carotenoids (lycopene, α-carotene, 13Z-β-carotene, (all-E)-β-carotene, 9Z-β-carotene, lutein, β-cryptoxanthin, zeaxanthin, antheraxanthin, and violaxanthin) were analyzed by high-performance liquid chromatography (HPLC; Agilent 1100 series, Agilent, Massy, France) as previously described in detail (Ha et al., 2019; You et al., 2020). Free phenolic acids (*p*-hydroxybenzoic acid, vanillic acid, *p*-coumaric acid, ferulic acid, and sinapic acid) were analyzed by a gas chromatograph-mass spectrometer (GC-MS; GCMS-QP2010 Ultra System, Shimadzu, Kyoto, Japan) as previously described (Kim et al., 2017). The data were calculated by using Student's *t*-test in Microsoft Excel, and differences were considered significant at $p < 0.001$ (***), $p < 0.01$ (**), or $p < 0.05$ (*).

2.5. Metabolomics of hydrophilic and lipophilic compounds

Hydrophilic compounds, including sugars, organic acids, aromatic acids, amino acids, and amino acid derivatives, were extracted from the powered rice seed samples as described in a previous study (Kim et al., 2017). The metabolites were separated using a 6890N GC system (Agilent) coupled to a Pegasus HT time-of-flight MS (TOF-MS; LECO, St. Joseph, MI). An in-house library was used to identify the metabolites. The peak area was calculated for relative quantification to the internal standard. Lipophilic compounds, including tocopherols, phytosterols, and policosanols, in the powered rice seed samples were also extracted as previously described (Kim et al., 2015). Identification was carried out by using a GC-MS, and contents were calculated using calibration curves. To visualize the metabolite changes, the free open-source program PathVisio 3.3.0 (https://www.pathvisio.org; Kutmon et al., 2015) was used in conjunction with the biological pathway of *Arabidopsis* from the AtMetExpress overview (https://www.wikipathways.org/index.php/). Data were calculated as log2 fold changes compared with the values at 60 days after flowering (DAF) of NT. The metabolite names were converted into PubChem compound IDs (PubChem CIDs) for input into PathVisio program.

2.6. Quantification of starch, sucrose, lysine, threonine, and γ-aminobutyric acid and measurement of carbon-to-nitrogen ratio

For further quantification, starch contents were measured using a starch assay kit (STA20, Sigma-Aldrich). The concentration of sucrose, lysine, threonine, and γ-aminobutyric acid (GABA) were calculated using calibration curves that were made for each standard through separation using a 7890B GC system (Agilent) coupled to a Pegasus BT TOF-MS system (LECO) for sucrose and threonine and a 6890N GC system (Agilent) coupled to a Pegasus HT TOF-MS system (LECO) for lysine and GABA as previously described in detail (Kim et al., 2017). The percentage of carbon and nitrogen contents was measured by elemental analyzer (FlashSmart Elemental Analyzer, Thermo Scientific) to calculate carbon-to-nitrogen (C/N) ratio of the fully mature and dried seeds. The data were analyzed by using Student's *t*-test in Microsoft Excel, and differences were considered significant at $p < 0.001$ (***), $p < 0.01$ (**), or $p < 0.05$ (*).

2.7. Transmission electron microscopy

Rice leaves at 150 DAG (days after germination) and immature rice seeds at 25 and 30 DAF were harvested from the paddy field and used for transmission electron microscopy (TEM). Samples were prepared from the second vein region of leaves and the central region of seeds in the longitudinal direction. Each sample was washed with phosphate-buffered saline (pH 7.4), prefixed with 2.5% glutaraldehyde for 12 h, and postfixed with 2% (w/v) osmium tetroxide for 2 h. After dehydration, the samples were sequentially imbedded into EMbed 812 resin (EMS, Hatfield, PA), polymerized into blocks for 3 days, and then sectioned by an ultramicrotome (Leica EM UC6; Leica, Nussloch, Germany) to an 80 nm thickness. After each specimen was stained with 2% uranyl acetate for 10 min and Reynolds lead citrate for 2 min, images were taken by a Tecnai G2-20 S-Twin device (FEI Company, Hillsboro, OR) in a TEM grid.

3. Results

3.1. Blue light-inducible OsMYBR22 is an OsRVE1 belonging to the CCA1-like subfamily

To affirm the characteristics of *OsMYBR22* as a blue light-inducible gene that has been predicted in our previous study (Lakshmanan et al., 2015), rice seedlings were grown under two different light conditions. Compared with white light, blue light increased the total

contents of two photosynthetic pigments, chlorophylls (1.4-fold) and carotenoids (1.3-fold), and the expression level of the *OsMYBR22* gene (3.4-fold) (Fig. 1A and B and Supplementary Table S2).

To better understand the molecular information of the OsMYBR22, its full-length amino acid sequences were subjected to multiple alignments among plant MYB-related proteins from the NCBI sequence database (http://blast.ncbi.nlm.nih.gov/Blast.cgi) with the Clustal-W algorithm of the MegAlign program (DNASTAR Lasergene, Madison, WI). The phylogenetic tree was constructed with 24 homologs of the CCA/LHY/RVE family using the Molecular Evolutionary Genetics Analysis (MEGA) 6 software. Blue light-inducible expression patterns were then applied using two previous microarray data sets for rice and *Arabidopsis* (Jiao et al., 2005; Lakshmanan et al., 2015) as shown in Fig. 1C. The tree displays two subfamilies, CCA1-like and LHY-CCA1-like. Four rice proteins including OsMYBR22 were clustered within a CCA1-like subfamily along with two *Brachypodium* (*Brachypodium distachyon*), two maize (*Zea mays*), and six *Arabidopsis* proteins. The OsMYBR22 more closely clustered to BdRVE1, ZmMYBR52/ZmRVE1, OsMYB511/OsRVE2, AtRVE1, and AtRVE2 in this order and clustered distantly to OsRVE3 and OsCCA1/OsLHY. Given the relatively high sequence similarity of OsMYBR22 with that of several RVE1s, the strongly inducible gene expression property between *OsMYBR22* and *AtRVE1* under blue light suggests a possible function of OsMYBR22 as an RVE1 orthologous protein in rice, an OsRVE1.

To compare diurnal and circadian gene expression profiles among the four rice CCA1-like subfamily genes, publicly available *in silico* data sets from RiceXPro (https://ricexpro.dna.affrc.go.jp/RXP_0002/index.php) were investigated (Fig. 1D). Interestingly, the four genes showed sequential diurnal rhythms with approximately 2-h intervals among *OsMYBR511/OsRVE2*, *OsMYBR22/OsRVE1*, *OsRVE3*, and *OsCCA1/OsLHY* in this order. This result suggested different and unique roles of these genes despite their close relationship as homologs of OsCCA1/OsLHY, the major core clock gene.

3.2. Overexpression of OsMYBR22 exhibits a stay-green phenotype in rice plants

To investigate the role of *OsMYBR22 in planta*, *GFP*-fused and *Myc*-tagged *OsMYBR22* vectors were constructed for subcellular localization and constitutive overexpression, respectively (Supplementary Fig. S1A). The two GFP fusion proteins, OsMYBR22:sGFP and eGFP:OsMYBR22 commonly displayed green fluorescence in the nucleus of rice protoplasts (Supplementary Fig. S1B) and two Myc-tagged proteins, OsMYBR22:Myc and Myc:OsMYBR22, abundantly accumulated in seven transgenic rice plants when immunoblotting was examined with an anti-Myc antibody (Supplementary Fig. S1C). Five independent lines were confirmed to have a single T-DNA copy number in the heterozygotic T_0 generation (Supplementary Fig. S1D). Two lines, OsMYBR22:Myc #8 (a

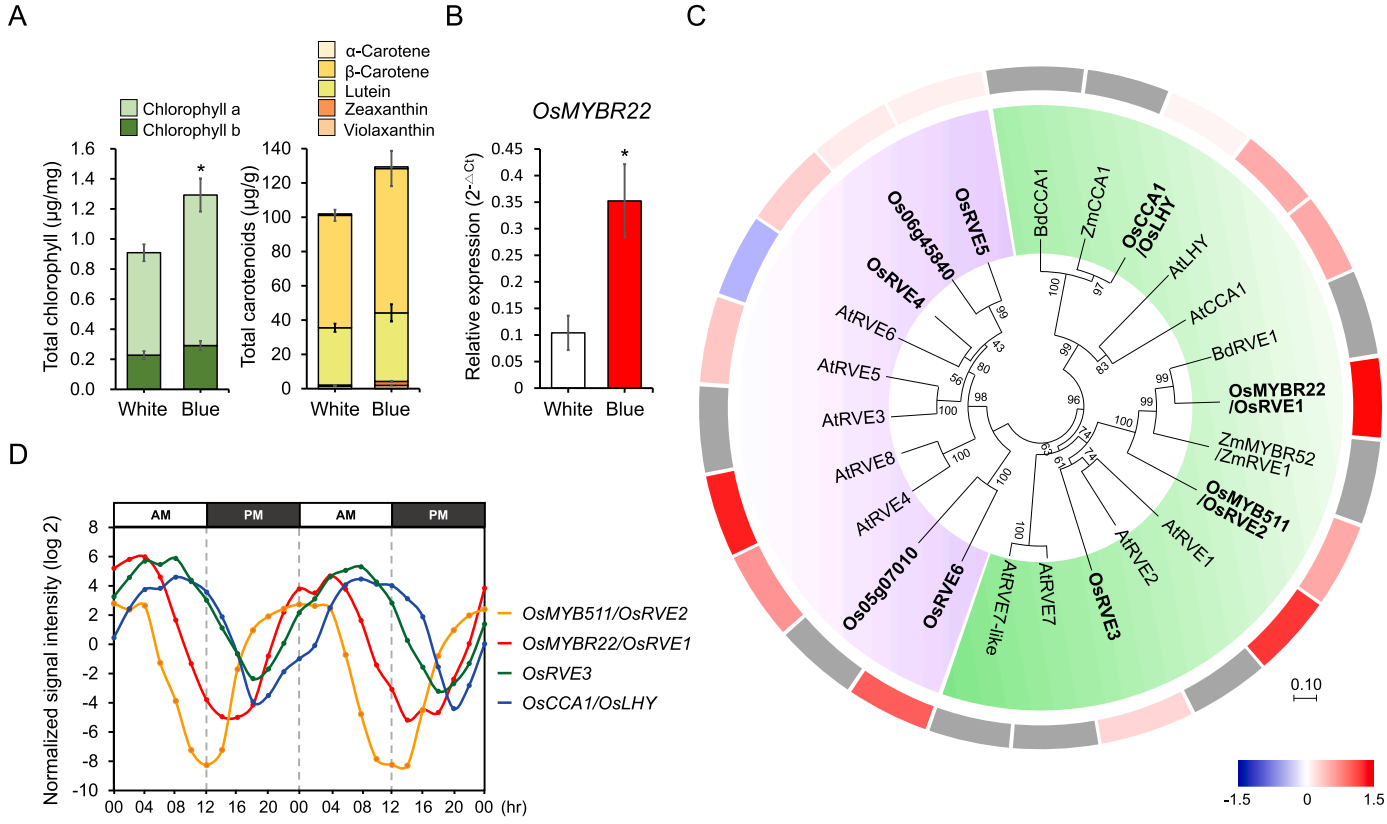

Fig. 1. Effects of blue light illumination on concentration of photosynthetic pigments, *OsMYBR22* expression, and molecular analysis of the phylogenetic tree and diurnal rhythm among OsMYBR22 homologs belonging to the CCA/LHY/RVE family. (A) Contents of chlorophylls and carotenoids between white and blue light treatments in leaf blades. The original analytical values for chlorophyll and carotenoids are shown in Supplementary Table S2 (B) Expression levels of *OsMYBR22* between white and blue light treatments by quantitative real-time PCR in leaf blade. (C) Phylogenic tree of 24 OsMYBR22 homologs comprising 9 rice (*Oryza sativa*), 2 *Brachypodium* (*Brachypodium distachyon*), 2 maize (*Zea mays*), and 11 *Arabidopsis* proteins belonging to the CCA/LHY/RVE family; further classification into two subfamilies of CCA1-like (in green background) and LHY-CCA1-like (in purple background) genes. The *in silico* blue/white expression heat map was visualized as the log2 fold change using two previous microarray data sets of rice (Lakshmanan et al., 2015) and *Arabidopsis* (Jiao et al., 2005). The gray boxes indicate absence of gene expression information from the microarray database. (D) Reconstruction of *in silico* diurnal expression profiles with the RiceXPro data set (https://ricexpro.dna.affrc.go.jp/RXP_0002/index.php) for four rice CCA1-like subfamily genes, *OsMYB511/OsRVE2* (Os04g49450), *OsMYBR22/OsRVE1* (Os02g46030), *OsRVE3* (Os06g51260), and *OsCCA1/OsLHY* (Os08g06110). (For interpretation of the references to color in this figure legend, the reader is referred to the Web version of this article.)

C-terminal Myc-tagged line, C8) and Myc:OsMYBR22 #11 (an N-terminal Myc-tagged line, N11), were chosen for further study as representative *OsMYBR22*-overexpression (*OsMYBR22*-OX) plants based on the increased expression levels of *OsMYBR22* in the homozygotic T_3 generation (Supplementary Fig. S1E).

To reveal the effects of *OsMYBR22* on rice leaf physiology, two homozygous *OsMYBR22*-OX lines were grown in paddy fields. We observed their phenotypes, examined the gene expression, and analyzed the pigment contents at 150 DAG of the reproductive stage (Fig. 2). *OsMYBR22*-OX plants showed darker green leaf color and shorter height (80% and 84% levels in C8 and N11, respectively) relative to NT plants, despite similar leaf blade lengths, implying a shorter sheath (Fig. 2A and B). Overexpression of the *OsMYBR22* was verified with high levels of transgene and total expression and repressed endogenous *OsMYBR22* expression at two diurnal time points (Fig. 2C). Interestingly, the *OsMYBR22* transgene, which was constitutively expressed under PGD1 promoter, showed similar oscillation pattern that endogenous *OsMYBR22* did: high in ZT01 compared to low ZT13. It was similar phenomenon in previous reports corresponding to *AtCCA1* (Yakir et al., 2007) and *OsCCA1* (Wang et al., 2020), suggesting the similar regulatory mechanism of CCA1-like family. To find out which pigments caused the darker leaf color, levels of chlorophylls, carotenoids, and phenolic compounds were analyzed (Fig. 2D and Supplementary Table S3). Results showed higher concentration of total chlorophylls (1.5- and 1.7-fold) and carotenoids (1.6- and 1.7-fold with 1.3- and 1.1-fold higher β/α ratio) in C8 and N11 plants, respectively, but slightly lower contents

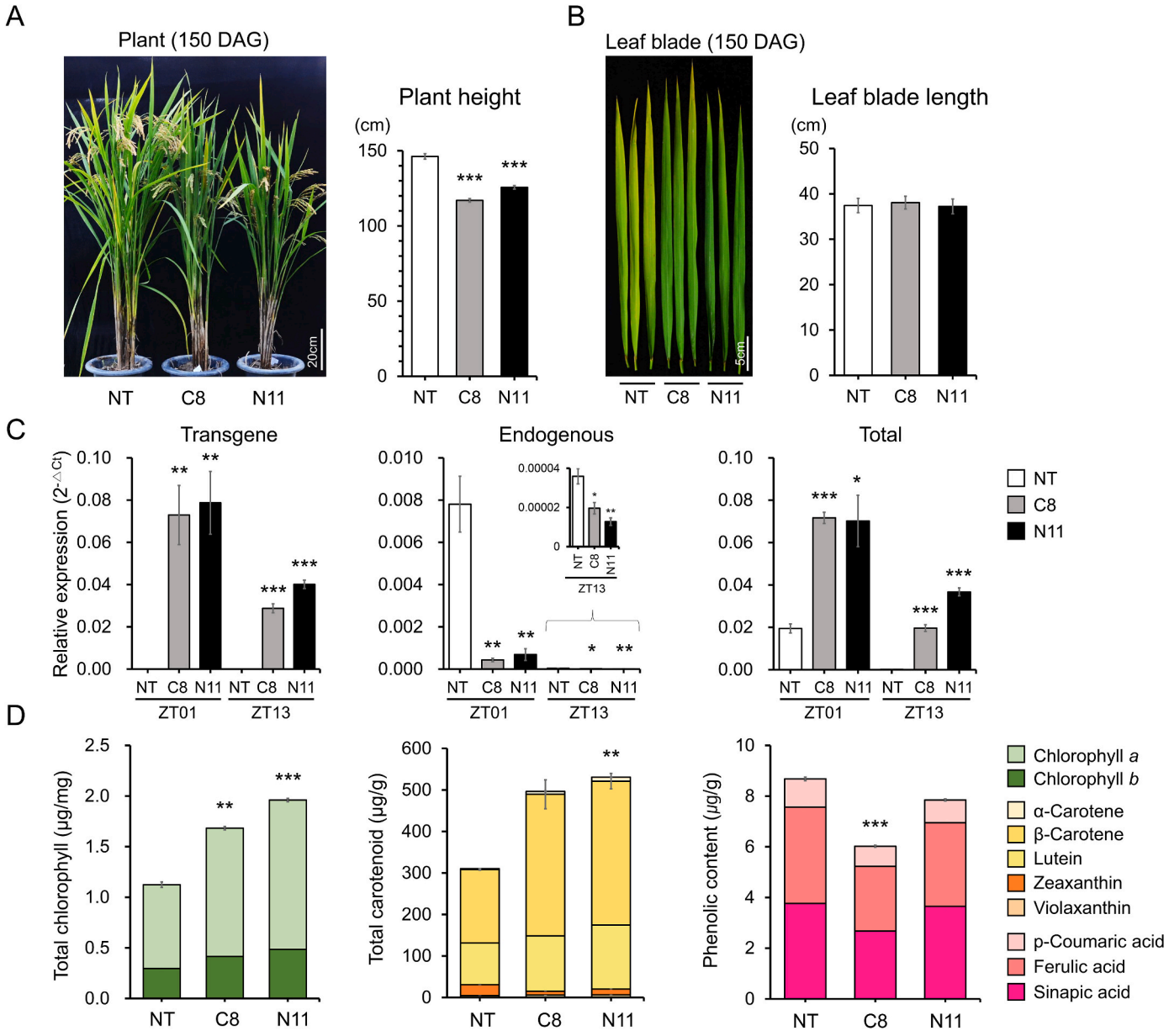

Fig. 2. Effects of *OsMYBR22* overexpression on rice leaf phenotypes. (A) Images of plants and a bar graph of plant height (n = 9) at 150 days after germination (DAG) between nontransgenic (NT) and two *OsMYBR22*-overexpressing transgenic (C8 and N11) plants. (B) Images of flag leaves and a bar graph of leaf blade length (n = 13) at 150 DAG among NT, C8, and N11 plants. (C) Expression levels of *OsMYBR22* examined at two diurnal points of zeitgeber time (ZT) 0 and ZT 13 in flag leaves (n = 4) at 150 DAG by quantitative real-time PCR using primer sets (listed in Supplementary Table S1) for transgene-specific, endogenous gene-specific, and common genes among NT, C8, and N11 plants. (D) Contents of pigment metabolites, including chlorophylls, carotenoids, and phenolics, of flag leaves (n = 3) by HPLC at 150 DAG among NT, C8, and N11 plants. All statistical significance was analyzed by using Student's *t*-test (***, $p < 0.001$; **, $p < 0.01$; *, $p < 0.05$). The original analytical values for chlorophyll and carotenoids are shown in Supplementary Table S3.

of phenolic compounds in both transgenic plants relative to NT plants. These results suggested that ectopic expression of *OsMYBR22* resulted in a shorter plant height and stay-green leaves due to enhanced levels of chlorophylls and carotenoids.

3.3. Overexpression of OsMYBR22 represents an everlasting green phenotype in rice grains

To unravel the influences of *OsMYBR22* on rice seed physiology, color phenotypes, and gene expression, pigment content was examined during maturation. Agronomic traits and germination rate were evaluated after harvest of T_4 homozygous *OsMYBR22*-OX seeds (Fig. 3). The green color was displayed at 30 DAF, when it had completely disappeared in NT seeds, and lasted until maturity at 60 DAF in *OsMYBR22*-OX seeds (Fig. 3A). Ectopically high expression of the *OsMYBR22* was also confirmed throughout the seed development with relatively higher expression in earlier stages and repressed endogenous *OsMYBR22* expression, which was low and gradually increased toward later stages in NT seeds (Fig. 3B). To determine the influence of pigments on the prolonged green color in grains, the concentration of chlorophylls, carotenoids, and phenolic compounds were quantified (Fig. 3C and Supplementary Table S4). Chlorophylls were present at 30 DAF in large

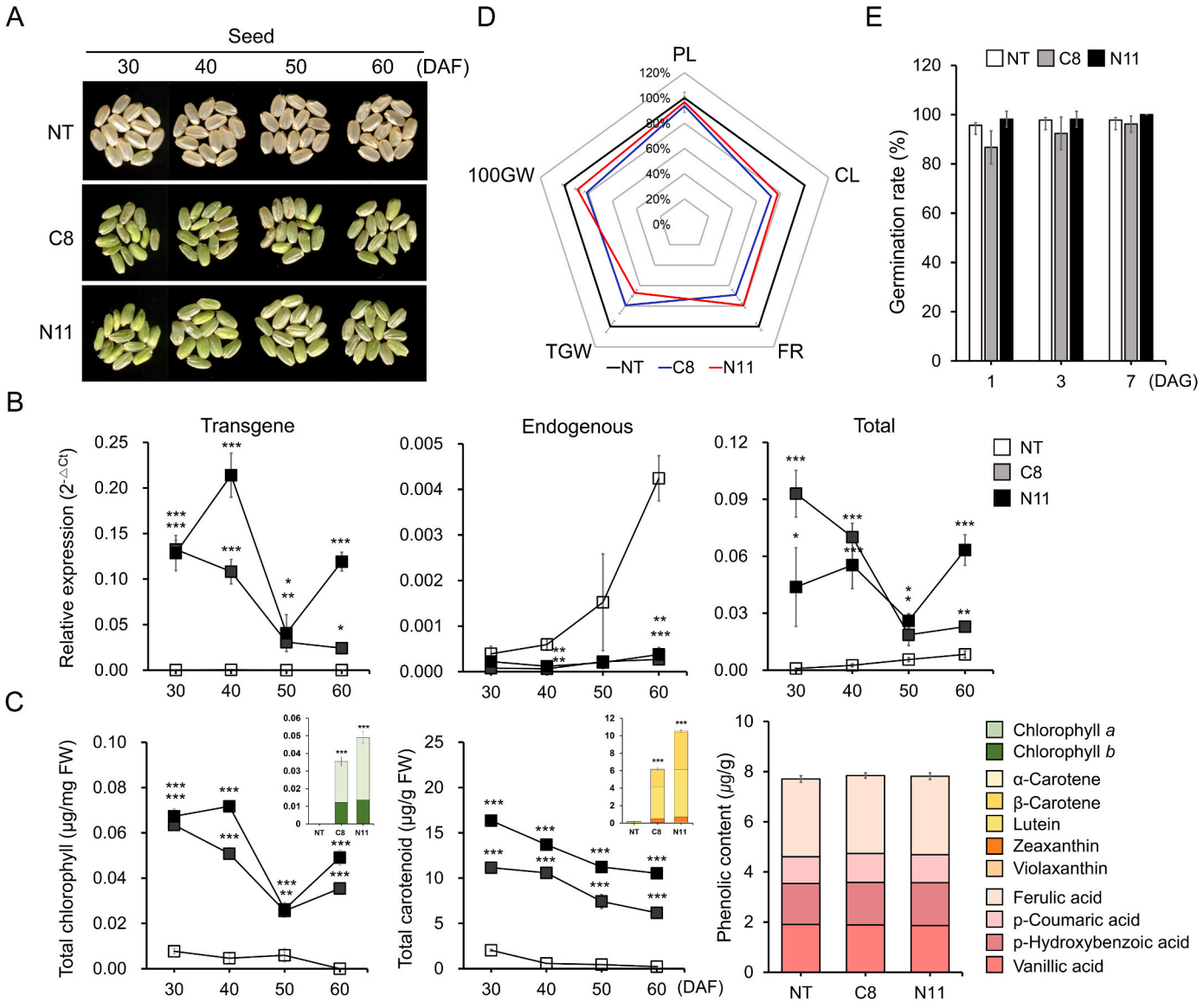

Fig. 3. Effects of *OsMYBR22* overexpression on rice seed phenotypes. (A) Images of seeds showing the color difference after dehusking during development at 30, 40, 50, and 60 days after flowering (DAF) between nontransgenic (NT) and two *OsMYBR22*-overexpressing transgenic (C8 and N11) plants. (B) Expression levels of *OsMYBR22* examined in the regions of transgene-specific, endogenous gene-specific, and common genes on 30, 40, 50, and 60 DAF seeds (n = 3) by quantitative real-time PCR among NT, C8, and N11 plants. The error bars represent the standard deviations of three replicate experiments. The primers used are listed in Supplementary Table S1 (C) Chlorophyll and carotenoid contents at 30, 40, 50, and 60 DAF seeds (n = 3) and phenolic content at 60 DAF seeds (n = 3) among NT, C8, and N11 plants. Particularly, individual component of chlorophylls and carotenoids at 60 DAF seeds was represented as small bar graphs to show the content ratio. All statistical significance was calculated via two-tailed Student's *t*-test (***, $p < 0.001$; **, $p < 0.01$; *, $p < 0.05$). The original analytical values for chlorophylls and carotenoids are shown in Supplementary Table S4 (D) Spider plot displaying mean values compared to 100% levels of NT seeds for approximately five major agronomic traits: panicle length (PL), culm length (CL), filling rate (FR), total grain weight (TGW), and 100-grain weight (100 GW), of C8 and N11 seeds at the fully mature and dried stages (n = 30 in the T_4 generation). Original box plots for all eight agronomic traits are shown in Supplementary Fig. S2 (E) Bar graph showing the germination rate examined for fully mature and dried seeds (n = 20) during 1 week among NT, C8, and N11 plants. (For interpretation of the references to color in this figure legend, the reader is referred to the Web version of this article.)

quantities in C8 (6-fold) and N11 (7-fold) seeds and remained even at 60 DAF in transgenic seeds relative to NT seeds, in which chlorophylls were absent since 30 DAF. Carotenoid contents were also considerably higher throughout seed maturation in C8 (5-, 19-, 16-, and 28-fold with increased β/α ratio of 1.2-fold at 60 DAF) and N11 (8-, 24-, 25-, and 48-fold with increased β/α ratio of 1.6-fold at 60 DAF) than in those four stages of NT seeds. In addition, the levels of phenolic compounds did not significantly change. Interestingly, the patterns of increased chlorophyll contents were concordant with transgene expression profiles during seed development, suggesting obvious effects by *OsMYBR22*-OX to the accumulation of chlorophylls rather than carotenoids (Fig. 3B and C).

Meanwhile, the levels of agronomic traits were decreased for five parameters, PL (94 and 97%), CL (72 and 78%), FR (69 and 79%), TGW (79 and 67%), and 100 GW (81 and 89%), in C8 and N11 seeds, respectively, and not significantly for the other three parameters, TNG, NP, and NSP, compared to the 100% levels of the NT seeds (Fig. 3D and Supplementary Fig. S2). Despite reduced grain yield qualities, the *OsMYBR22*-OX seeds had fully germinated at 7 days after imbibition without significant change (Fig. 3E).

3.4. Transcriptional influences on the chlorophyll- and carotenoid-associated genes by overexpression of OsMYBR22

To identify whether *OsMYBR22* transcriptionally modulates the photosynthetic pigment metabolisms, the expression levels of 40 endogenous genes involving rice CCA1-like subfamily (4), chlorophyll biosynthesis (9), chlorophyll degradation (11), and carotenoid biosynthesis (16), as represented by their known functions and regulatory relationships in the schematic pathways of Supplementary Fig. S3, were examined in the leaves at 150 DAG and seeds during development (Fig. 4). Most noticeably except *OsMYBR22/OsRVE1* that was overexpressed, the transcript levels of all CCA1-like subfamily and chlorophyll biosynthesis-associated genes were lower in *OsMYBR22*-OX than NT seeds in late maturing stages (Fig. 4A, Supplementary Fig. S4B). They

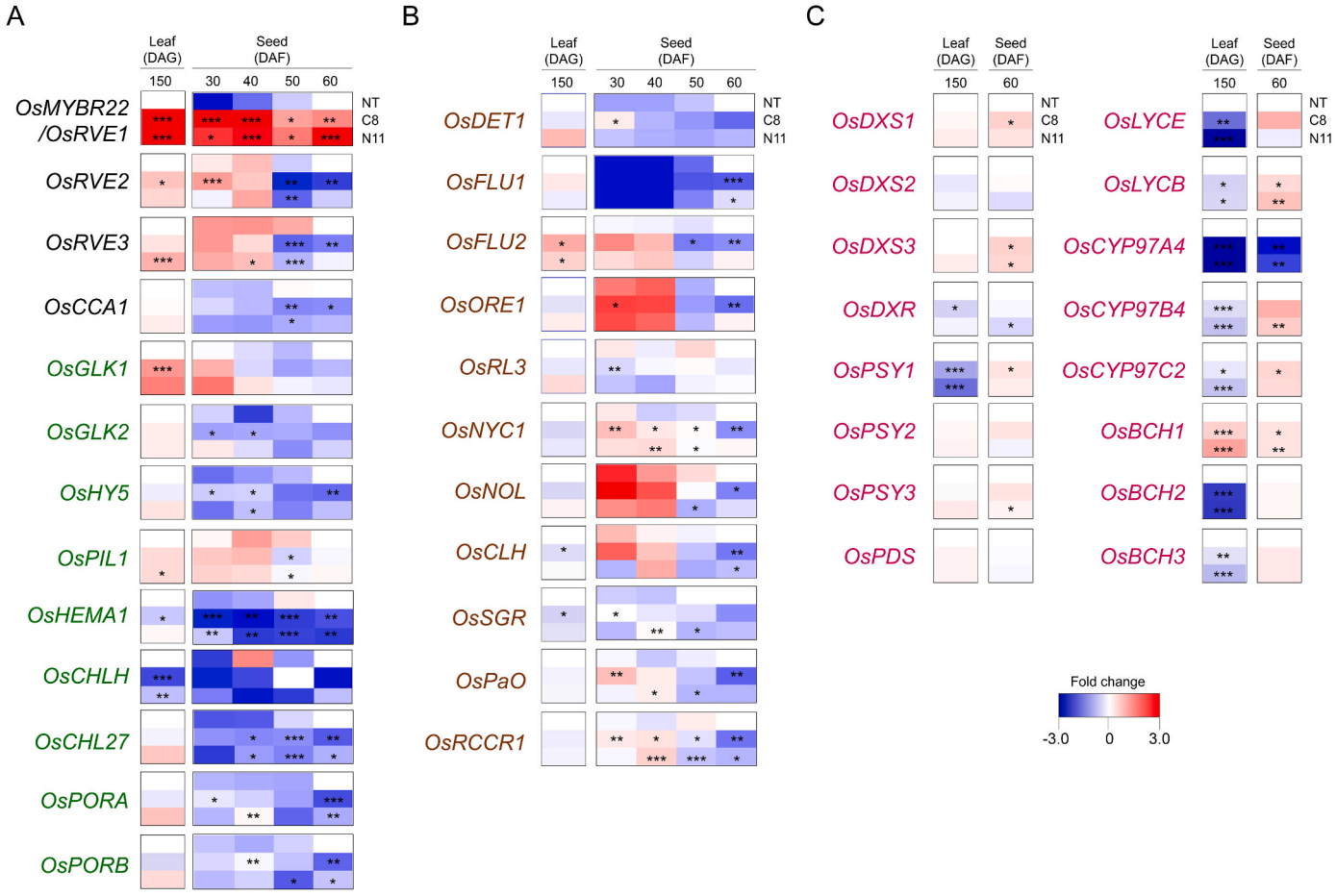

Fig. 4. Heat map of the expression levels of chlorophylls and carotenoid metabolic genes between NT and *OsMYBR22*-OX lines. The qRT-PCR analysis was performed for 40 genes, including (A) four CCA1-like subfamily and nine chlorophyll biosynthesis-associated genes, (B) eleven chlorophyll degradation-associated genes, and (C) 16 carotenoid biosynthetic pathway genes. Their known functions and regulatory relationships are marked in the schematic pathways for chlorophylls and carotenoid metabolism in Supplementary Fig. S3. The original bar and line graphs displaying the qRT-PCR results are shown in Supplementary Figs. S4A–F. All statistical significances were calculated via two-tailed Student's *t*-test (***, $p < 0.001$; **, $p < 0.01$; *, $p < 0.05$). Each primer sequence is provided in Supplementary Table S1. The abbreviations of genes encoding the following regulatory TFs and enzymes are as follows: OsRVE, rice REVEILLE; OsCCA1, rice CIRCADIAN CLOCK-ASSOCIATED1; OsGLK, rice GOLDEN2-LIKE; OsHY5, rice ELONGATED HYPOCOTYL5; OsPIL1, rice phytochrome-interacting factor-like1; OsHEMA, rice glutamyl-tRNA reductase; OsCHLH1, rice Mg-chelatase subunit H; OsCHL27, rice aerobic Mg-protoporphyrin IX monomethyl ester oxidative cyclase; OsPORA and B, rice NADPH:protochlorophyllide oxidoreductase A and B; OsDET1, rice DE-ETIOLATED1; OsFLU, rice FLUORESCENT; OsORE1, rice ORESARA1-like1; OsRL3, rice RADIALIS-LIKE3; OsNYC1, rice NON-YELLOW COLORING1; OsNOL, rice NYC1-LIKE; OsCLH, rice chlorophyllase; OsSGR/OsNYE, rice STAY-GREEN/NON-YELLOWING/Mg-dechelatase; OsPaO, rice pheophorbide a oxygenase; OsRCCR1, rice red chlorophyll catabolite reductase1; OsDXS, rice 1-deoxy-d-xylulose-5-phosphate synthase; OsDXR, rice 1-deoxy-d-xylulose 5-phosphate reductoisomerase; OsPSY, rice phytoene synthase; OsPDS, rice phytoene desaturase; OsLCYE, rice lycopene ε-cyclase; OsLCYB, rice lycopene β-cyclase; OsCYP97A4, rice cytochrome P450-type β-carotene hydroxylase 97A4; OsCYP97B4, rice cytochrome P450-type β-carotene hydroxylase 97B4; OsCYP97C2, rice cytochrome P450-type ε-carotene hydroxylase 97C2; OsBCH, rice non-heme di-iron type β-carotene hydroxylase. (For interpretation of the references to color in this figure legend, the reader is referred to the Web version of this article.)

exhibited opposite patterns as the seeds mature: we observed a decrease in *OsMYBR22*-OX seeds, which have abundant chlorophylls, but an increase in NT seeds, which lack chlorophylls. This result strongly implies the existence of a feedback regulatory mechanism for chlorophyll biosynthesis in rice seeds. On the other hand, *OsRVE2*, *OsRVE3*, *OsGLK1*, and *OsPIL1* transcripts were upregulated in the leaves and early seeds by *OsMYBR22*-OX, speculating that their contribution for the enhanced levels of chlorophylls in the leaves and early maturing seeds. In cases of chlorophyll degradation-associated genes, two genes in the leaves, *chlorophyllase* (*OsCLH*) and *STAY-GREEN* (*OsSGR*), and all genes in the late maturity seeds were significantly downregulated, suggesting that their repression might be involved in the prolonged chlorophyll contents (Fig. 4B and Supplementary Figs. S4C and S4D).

Carotenoid biosynthetic gene expressions showed overall different patterns for up- and downregulation between two organs: one and nine genes in the leaves and eight and two genes in the seeds, respectively (Fig. 4C and Supplementary Figs. S4E and S4F). Common patterns in both organs were the downregulation of *OsCYP97A4*, which encodes a β-ring hydroxylase preferring α-carotene substrate, and the upregulation of *OsBCH1*, which encodes a β-ring hydroxylase preferring β-carotene substrate, with significance. It suggested that the enhanced levels of carotenoids in the leaves and seeds of the *OsMYBR22*-OX lines might not

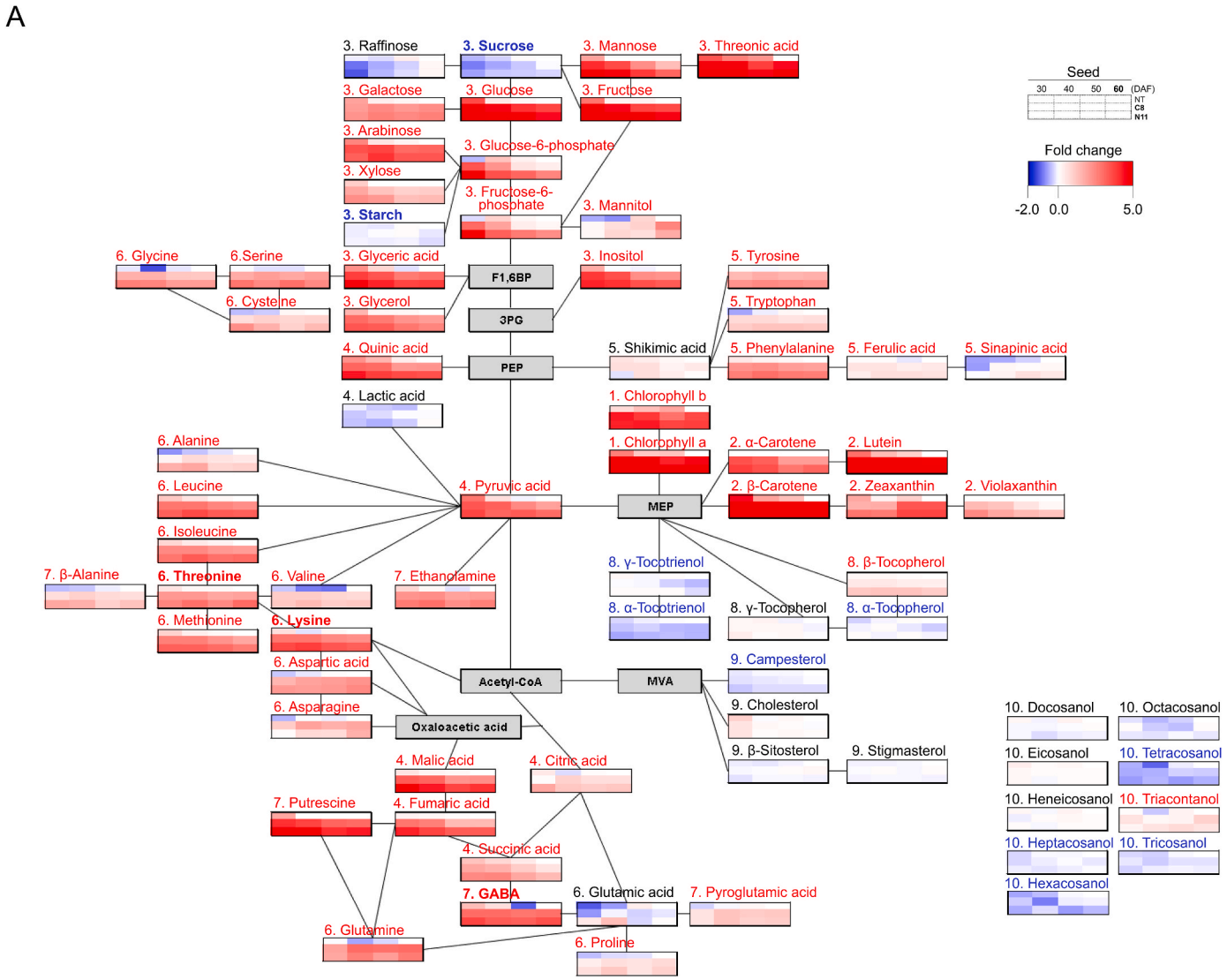

Fig. 5. Metabolite analysis during seed development and fully matured and dried seed color phenotypes between NT and EGR lines. (A) Heat map showing differences in 74 metabolites in the schematic pathway between NT and 2 *OsMYBR22*-OX lines at 4 seed developmental stages, 30, 40, 50, and 60 DAF, using a metabolomics approach. Each value was calculated as the log2 fold change compared with the level of NT seeds at 60 DAF. The different colors of metabolite names in red (increase) and blue (decrease) showed consistent patterns in two *OsMYBR22*-OX seeds. Unchanged metabolites are in black. The original analytical values and bar graphs displaying the results are shown in Supplementary Tables S3–5. The number in front of each metabolite name represents the classification groups. The gray boxes represent the metabolites below detection level. The abbreviations are as follows: F1,6BP, fructose-1,6-bisphosphate; 3 PG, 3-phosphoglyceric acid; PEP, 2-phosphoenolpyruvate; MEP, mevalonate; MVA, mevalonic acid. (B) Pie charts showing the total contents of ten groups of metabolites in fully matured 60 DAF seeds, respectively: 1, chlorophylls; 2, carotenoids; 3, sugars; 4, organic acids; 5, aromatic acids and aromatic amino acids; 6, amino acids; 7, amino acid derivatives; 8, tocols; 9, phytosterols; and 10, policosanols. Relative proportion displayed as size of circle based on the total content of each group in N11 line that set to 100%. Statistical significance of each metabolite is marked with asterisks with colors, red for increase and blue for decrease, in the next to the name. (C) Quantification of two dietary and three nutritional metabolites considered important in rice grains as foods and feeds. The metabolites were analyzed in fully matured seeds at 60 DAF. (D) Carbon/nitrogen (C/N) ratio by quantification of carbon and nitrogen contents with the same fully matured seeds. (E) Images of 100 unpolished seeds at the fully matured and dried stages to compare color phenotypes between NT and EGR. All statistical significances were calculated via two-tailed Student's t-test (***, $p < 0.001$; **, $p < 0.01$; *, $p < 0.05$). (For interpretation of the references to color in this figure legend, the reader is referred to the Web version of this article.)

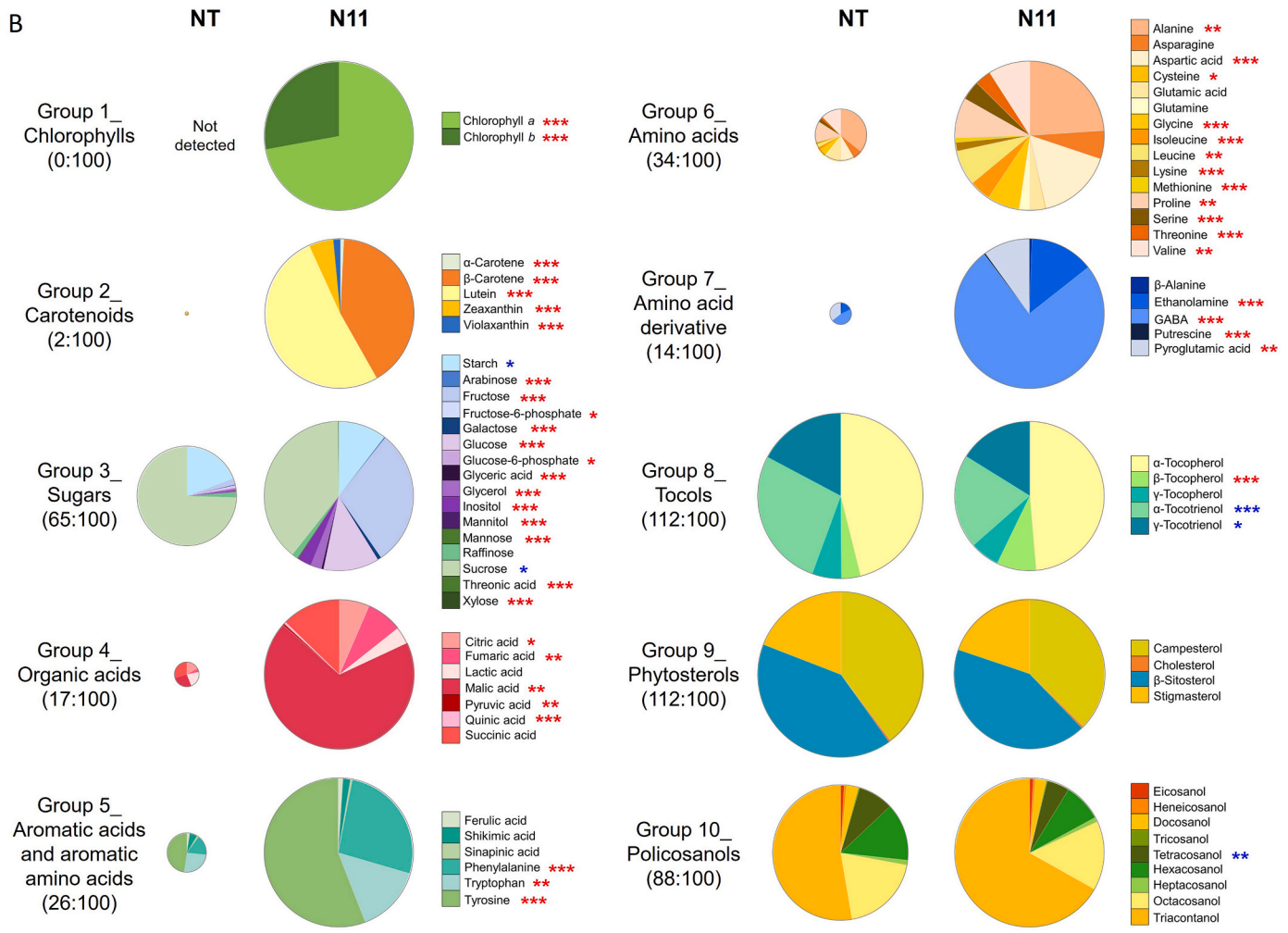

Fig. 5. (*continued*).

be influenced by the transcriptional upregulation of carotenoid biosynthetic genes. Instead, *OsMYBR22*-OX could affect the distribution with a preference toward β-carotenoids in the carotenoid biosynthetic pathway, supported by a higher β/α ratio, as shown before in the leaves and seeds (Supplementary Tables S3 and S4).

3.5. Nutritional and functional metabolites are largely enhanced in rice grains by overexpression of OsMYBR22

We used a metabolomics approach during seed development to define the metabolic changes in *OsMYBR22*-OX seeds, which displayed an everlasting green phenotype (Fig. 5). A total of 74 metabolites including chlorophylls, carotenoids, and the other 8 groups of hydrophilic and lipophilic compounds were analyzed and illustrated the relative levels based on NT seeds at 60 DAF in the metabolic pathway (Fig. 5). Throughout developmental stages in *OsMYBR22*-OX seeds, 52 metabolites were increased: all 7 chlorophyll and carotenoid components, 13 out of 16 sugars, 6 out of 7 organic acids, 2 out of 3 aromatic acids, 17 out of 18 amino acids, all 5 amino acid derivatives, 1 out of 5 tocols, and 1 out of 9 policosanols. The remaining 22 metabolites decreased or did not significantly change (Fig. 5A and Supplementary Tables S4, S5, and S6). Pie charts showed the enhancement in total content of chlorophylls, carotenoids (47.9-fold), sugars (1.5-fold), organic acids (6.0-fold), aromatic metabolites (3.8-fold), amino acids (2.9-fold), amino acid derivatives (7.0-fold), and policosanols (1.1-fold) and the slight decrease in those of tocols (0.9-fold) and phytosterols (0.9-fold) in N11 seeds as a representative line (Fig. 5B).

To verify the value of the grain as a staple food crop, the dietary (starch and sucrose), nutritional (lysine and threonine), functional (GABA) metabolites, and carbon to nitrogen (C/N) ratio were quantitatively analyzed using unpolished T4 seeds that were harvested at 60 DAF, dried for a month, threshed, and dehusked. The contents showed the decreased levels of starch (0.9- and 0.8-fold) and sucrose (0.6- and 0.5-fold) and the largely increased levels of lysine (6.7- and 11.9-fold), threonine (3.44- and 8.6-fold), and GABA (5.7- and 8.0-fold) in C8 and N11 seeds, respectively, compared to NT seeds (Fig. 5C). Moreover, the decreased C/N ratio (0.8-fold), which caused by increasing nitrogen content (1.2-fold) without change of carbon content, reflected well the large increase in amino acids and amino acid derivatives of these edible grains (Fig. 5D). We designated a N11 line as a new biofortified variety, "Evergreen Rice (EGR)," with the best performance in nutritional and functional values of grain quality due to an everlasting green color (Fig. 5E).

3.6. Chloroplasts are structurally preserved in aging leaves and maturing seeds of EGR

To understand the anatomy of the greener phenotypes of *OsMYBR22*-OX plants, we performed TEM analysis on the leaves and seeds of EGR relative to NT rice (Fig. 6). The NT leaves begin to age at the

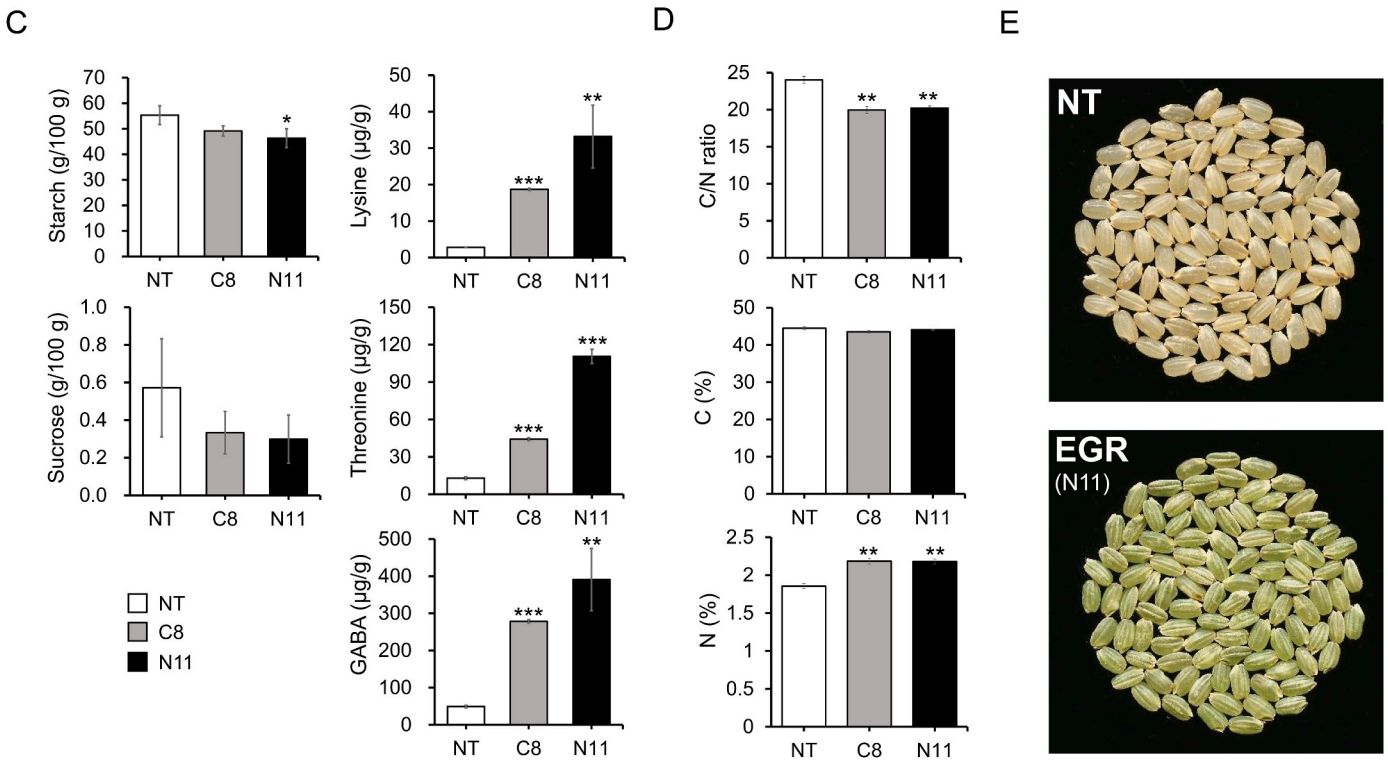

Fig. 5. (*continued*).

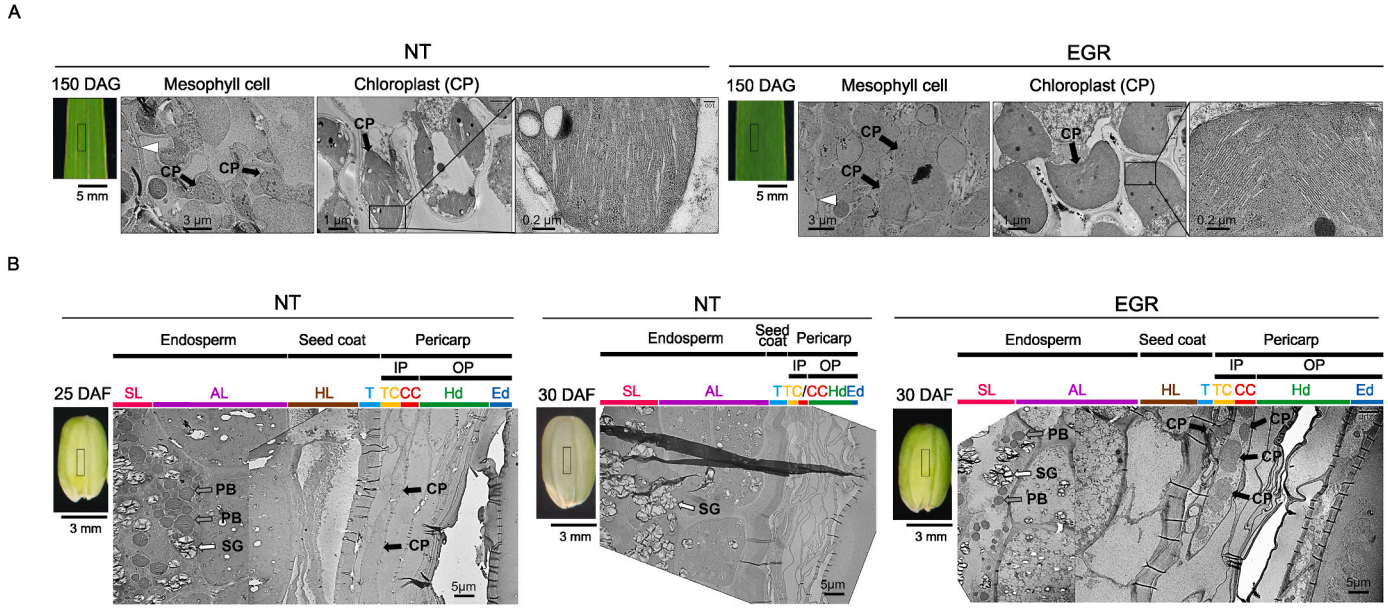

Fig. 6. Transmission electron microscopy of leaves and seeds between NT and EGR lines. (A) Leaf subcellular organelles were observed in rice flag leaves at 150 DAG, as shown in the black-squared region. Microphotographs displaying mesophyll cells located outside of bundle sheath cells marked with white triangles and sequentially magnified to look closer at chloroplasts and thylakoid stacking. (B) Seed subcellular organelle structures were observed using dehusked maturating seeds of NT at 25 DAF and 30 DAF and of EGR at 30 DAF, as shown in the black-squared region. Microphotographs showing the following four compartmentalized regions: endosperm, seed coat, inner pericarp (IP), and outer pericarp (OP). Each region includes more partitioned layers: the starch layer (SL) and aleurone layer (AL) in the endosperm, the hyaline layer (HL) and testa (T) in the seed coat, tubular cells (TC) and cross cells (CC) in the IP, and the hypodermis (Hd) and epidermis (Ed) in the OP. Chloroplasts (CP), protein bodies (PB), and starch grains (SG) are designated with arrows in black, gray, and white, respectively.

reproductive stage of 150 DAG by showing some cracks that signify chloroplast destruction in mesophyll cells; however, the EGR leaves have more chloroplasts that are intact and larger shapes with wider and thicker granum stacking in mesophyll cells (Fig. 6A). This result suggested significantly delayed senescence in the EGR leaves.

Our observation of EGR seed internal cell structures showed that by 30 DAF, the seed coat and pericarp have degenerated and degraded chloroplasts, removing the green color of NT seeds (Fig. 6B). To our surprise, the ERG seeds maintained the clearly delineated seed coat and pericarp structures, which included the hyaline layer and testa in the

seed coat, tubular cells and cross cells in the inner pericarp, and hypodermis and epidermis in the outer pericarp. Chloroplasts in the tubular and cross cells of the ERG seeds at 30 DAF stage showed even more developed and intact shapes than did those of the NT seeds at 25 DAF. The protein body structures in the starch layer that were usually absent in the NT seeds at 30 DAF were still observed in the EGR seeds at 30 DAF like in the NT seeds at 25 DAF. This result suggests that ripening processes were postponed for more than 5 days; therefore, the everlasting green color of the EGR might be caused by the structural retention of chloroplasts together with the prolonged chlorophyll accumulation even after harvest.

4. Discussion

Blue light was responsible for the increase in two photosynthetic pigments, chlorophylls and carotenoids, in rice plants (Fig. 1A). The overexpression of an *OsMYBR22*, which was induced under the blue light condition (Fig. 1B), caused similar phenotypes to those seen in responses to blue light signals of NT plants, weak dwarfing, greener leaf color, and increased amounts of chlorophylls and carotenoids (Fig. 2). A molecular phylogenetic tree with blue light-inducible patterns confirmed that *OsMYBR22* is the *OsRVE1* ortholog to plant *RVE1s* including *AtRVE1* and showed the close relation to three rice genes, *OsRVE2*, *OsRVE3*, and *OsCCA1/OsLHY*, as clock genes (Fig. 1C and D). The endogenous expression patterns have been reported for an *OsCCA1/OsLHY* as the main circadian clock gene (Shen et al., 2015) and for *OsMYBR22/OsRVE1* (same to *CMYB1*, Duan et al., 2014) and *OsRVE2* (same to *OsMYBR511*, Huang et al., 2015) with the cold-inducible profiles. Recently, it was shown that *OsCCA1/OsLHY* regulates tiller numbers, which increase by antisense suppression and decrease by overexpression (Wang et al., 2020) and fine-tunes the critical day length for photoperiodic flowering examined by genetic complementation of a late flowering mutant of *OsLHY*, *lem1*, and loss-of function approaches such as RNA interference and CRISPR/Cas9 in rice (Sun et al., 2021). However, the roles of rice CCA1-like family related to the greening phenotypes have never been studied. Instead, overexpression of *AtRVE1* showed higher greening rates of etiolated seedlings when exposed to light by promoting the transcription of only *AtPORA* among biosynthetic genes for protochlorophyllide, the intermediate in chlorophyll biosynthetic pathway (Xu et al., 2015). On the contrary, we found that overexpression of *OsMYBR22/OsRVE1* repressed the expressions of all examined chlorophyll biosynthesis-associating genes including *OsPORA* and prompted us to propose a feedback regulatory mechanism for chlorophyll biosynthesis in rice seeds (Fig. 4A). With the significantly repressed expression of almost chlorophyll degradation-associated genes in the late stages during seed maturation (Fig. 4B), the inhibition of chlorophyll degradation might be more responsible for the EGR trait rather than the reinforcement of chlorophyll biosynthesis. Considering our findings together with several *Arabidopsis* studies such as *AtCCA1* and *AtLHY* to maintain circadian rhythms with partial redundancy (Mizoguchi et al., 2002; Nagel et al., 2015), *AtCCA1* to inhibit leaf senescence (Song et al., 2018), and *AtRVE1* to positively control auxin levels during the day and repress phyB-mediated seed germination as one of the circadian systems (Rawat et al., 2009; Yang et al., 2020), we could speculate that the OsMYBR22/OsRVE1 might have distinctive roles from OsCCA1/OsLHY and other plant proteins belonging to CCA1-like family.

Intriguingly in this study, *OsMYBR22*-OX generated EGR traits that exhibit everlasting green color with highly prolonged contents of chlorophylls and carotenoids even after harvest beyond generations, and with the support of structurally preserved chloroplasts (Figs. 3A, 5D and 6B). Rice, the most important cereal species, is a staple food for over half of the world's population. It is rich in carbohydrates but particularly low in lysine and threonine among essential amino acids and destitute in micronutrients such as carotenoids as provitamin A components. Therefore, the strengthening nutritional value of rice has been a matter of great benefit to human health. Biofortification via plant biotechnology has independently improved the content and quality of nutrients and functional metabolites, including the carotenoids, lysine, and threonine, as recently summarized (Garg et al., 2018; Zhu et al., 2020). Several carotenoid-biofortified rice varieties, such as Golden Rice I (0.2 mg/100 g; Ye et al., 2000), Golden Rice II (3.7 mg/100 g; Paine et al., 2005), *stPAC* rice (0.4 mg/100 g; Jeong et al., 2017), and *OsDXS2-stPAC* rice (2.2 mg/100 g; You et al., 2020), have been engendered by different strategies. Also, high-lysine (1.4-fold) and high-threonine (1.2-fold) rice varieties were generated by overexpression of two artificial genes by fusing endogenous rice genes with lysine (K)/threonine (T) motif (TKTKK) coding sequences, but their contents were not quite high (Jiang et al., 2016). Moreover, GABA, a naturally occurring amino acid derivative that works as a neurotransmitter in the human brain, has been considered a bioactive target for mutant screening and conventional breeding of rice (Kim et al., 2013) and for biofortification by genome editing due to its blood pressure-lowering function in tomato (Nonaka et al., 2017). For this reason, a special Korean variety named "black waxy rice with a giant embryo" with high GABA contents (34 mg/100 g) has been considered as a raw material for mouse feeding experiments to examine attenuating obesity-associated metabolic disorders (Lee et al., 2016) and antianxiety effects (Jung et al., 2017). To surprisingly high levels, our EGR grains accumulated multiple valuable metabolites concurrently: chlorophylls (0.5 mg/100 g), carotenoids (1.1 mg/100 g), lysine (3.3 mg/100 g corresponding to 12-fold), threonine (11.1 mg/100 g corresponding to 9-fold), and GABA (39.1 mg/100 g) when compared to NT grains (Fig. 5C). Moreover, the contents of starch (46 g/100 g corresponding to 0.8-fold) and sucrose (0.3 g/100 g corresponding to 0.5-fold) as major sugar ingredients were considerably reduced in EGR relative to NT grains (Fig. 5C).

Indeed, metabolites that accumulated in the EGR grains are mainly biosynthesized from plastid-originated pathways. It is supportive that the structural integrity of chloroplasts as shown in Fig. 6B might have much more contribution beyond just preservation of chlorophylls. Therefore, EGR grains could simultaneously contain chloroplast-dependent metabolites. Eventually, we developed the new biofortified rice variety "EGR" by simultaneously accumulating multiple valuable phytonutrients, including chlorophylls (antioxidants), carotenoids (provitamin A), lysine and threonine (essential amino acids), and GABA (a dietary supplement effective at lowering blood pressure and reducing neuronal excitability) by the gain-of-function of *OsMYBR22/OsRVE1*. It has great potential to supply the highly improved nutritional and functional values for human as staple food grains.

Author statement

S-HH devised this study with S-HL and wrote the manuscript with YSJ, HC, and S-HL; YSJ and HC constructed the vectors, generated and cultivated the transgenic plants, and performed the molecular experiments; JKK and S-AB analyzed metabolites; M-KY performed the statistical analysis; DL contributed to the conceptual framework.

Data availability statement

The data supporting the findings of this study are available from the corresponding author, Sun-Hwa Ha, upon request.

Declaration of competing interest

The authors declare no competing financial interests.

Acknowledgments

This work was supported by grants from the Research Programs (NRF-2016R1A2B4013485 to S-HH and 2020R1I1A1A01073720 to HC) through the National Research Foundation of Korea funded by the

Ministry of Education, Science, and Technology. Our work was also supported by the New Plant Breed Technology Program (PJ01477202 to S-HH) funded by the Rural Development Administration, South Korea.

Appendix A. Supplementary data

Supplementary data to this article can be found online at https://doi.org/10.1016/j.ymben.2021.12.014.

References

Ambawat, S., Sharma, P., Yadav, N., Yadav, R., 2013. MYB transcription factor genes as regulators for plant responses: an overview. Physiol. Mol. Biol. Plants 19, 307–321.

Andronis, C., Barak, S., Knowles, S.M., Sugano, S., Tobin, E.M., 2008. The clock protein CCA1 and the bZIP transcription factor HY5 physically interact to regulate gene expression in *Arabidopsis*. Mol. Plant 1, 58–67.

Chen, Y., Yang, X., He, K., Liu, M., Li, J., Gao, Z., Lin, Z., Zhang, Y., Wang, X., Qiu, X., Shen, Y., Zhang, L., Deng, X., Luo, J., Deng, X.W., Chen, Z., Gu, H., Qu, L.-J., 2006. The MYB transcription factor superfamily of *Arabidopsis*: expression analysis and phylogenetic comparison with the rice MYB family. Plant Mol. Biol. 60, 107–124.

Chen, Y., Zhou, B., Li, J., Tang, H., Tang, J., Yang, Z., 2018. Formation and change of chloroplast-located plant metabolites in response to light conditions. Int. J. Mol. Sci. 19, 654.

Choi, H., Yi, T., Ha, S.-H., 2021. Diversity of plastid types and their interconversion. Front. Plant Sci. 12, 692024.

Christie, J.M., 2007. Phototropin blue-light receptors. Annu. Rev. Plant Biol. 58, 21–45.

De Wit, M., Galvão, V.C., Fankhauser, C., 2016. Light-mediated hormonal regulation of plant growth and development. Annu. Rev. Plant Biol. 67, 513–537.

Duan, M., Huang, P., Yuan, X., Chen, H., Huang, J., Zhang, H., 2014. CMYB1 encoding a MYB transcriptional activator is involved in abiotic stress and circadian rhythm in rice. Sci. World J., 178038, 2014.

Dubin, M.J., Bowler, C., Benvenuto, G., 2008. A modified gateway cloning strategy for overexpressing tagged proteins in plants. Plant Methods 4, 3.

Dubos, C., Stracke, R., Grotewold, E., Weisshaar, B., Martin, C., Lepiniec, L., 2010. MYB transcription factors in *Arabidopsis*. Trends Plant Sci. 15, 573–581.

Garg, M., Sharma, N., Sharma, S., Kapoor, P., Kumar, A., Chunduri, V., Arora, P., 2018. Biofortified crops generated by breeding, agronomy, and transgenic approaches are improving lives of millions of people around the world. Front. Nutr. 5, 12.

Gray, J., Bevan, M., Brutnell, T., Robin, B.C., Cone, K., Hake, S., Jackson, D., Kellogg, E., Lawrence, C., McCouch, S., Mockler, T., Moose, S., Paterson, A., Peterson, T., Rokshar, D., Souza, G.M., Springer, N., Stein, N., Timmermans, M., Wang, G., Grotewold, E., 2009. A recommendation for naming transcription factor proteins in the grasses. Plant Physiol. 149, 4–6.

Ha, S.-H., Kim, J.K., Jeong, Y.S., You, M.-K., Lim, S.-H., Kim, J.-K., 2019. Stepwise pathway engineering to the biosynthesis of zeaxanthin, astaxanthin and capsanthin in rice endosperm. Metab. Eng. 52, 178–189.

Hiei, Y., Ohta, S., Komari, T., Kumashiro, T., 1994. Efficient transformation of rice (*Oryza sativa* L.) mediated by *Agrobacterium* and sequence analysis of the boundaries of the T-DNA. Plant J. 6, 271–282.

Huang, P., Chen, H., Mu, R., Yuan, X., Zhang, H.S., Huang, J., 2015. OsMYB511 encodes a MYB domain transcription activator early regulated by abiotic stress in rice. Genet. Mol. Res. 14, 9506–9517.

Jeong, Y.S., Ku, H.-K., Kim, J.K., You, M.K., Lim, S.-H., Kim, J.-K., Ha, S.-H., 2017. Effect of codon optimization on the enhancement of the β-carotene contents in rice endosperm. Plant Biotechnol. Rep. 11, 171–179.

Jiang, S., Ma, A., Xie, L., Ramachandran, S., 2016. Improving protein content and quality by over-expressing artificially synthetic fusion proteins with high lysine and threonine constituent in rice plants. Sci. Rep. 6, 34427.

Jiao, Y., Ma, L., Strickland, E., Deng, X.W., 2005. Conservation and divergence of light-regulated genome expression patterns during seedling development in rice and Arabidopsis. Plant Cell 17, 3239–3256.

Johkan, M., Shoji, K., Goto, F., Hashida, S., Yoshihara, T., 2010. Blue light-emitting diode light irradiation of seedlings improves seedling quality and growth after transplanting in red leaf lettuce. Hortscience 45, 1809–1814.

Jung, E.S., Lee, S., Lim, S.-H., Ha, S.-H., Liu, K.-H., Lee, C.H., 2013. Metabolite profiling of the short-term responses of rice leaves (*Oryza sativa* cv. Ilmi) cultivated under different LED lights and its correlations with antioxidant activities. Plant Sci. 210, 61–69.

Jung, W., Kim, S., Lee, J., Kim, H., Son, B., Kim, J., Suh, J., 2017. Effect of feeding high gamma-aminobutyric acid-containing giant embryo black sticky rice (*Oryza sativa* L.) on anxiety-related behavior of C57BL/6 mice. J. Med. Food 20, 777–781.

Katiyar, A., Smita, S., Lenka, S.K., Rajwanshi, R., Chinnusamy, V., Bansal, K.C., 2012. Genome-wide classification and expression analysis of MYB transcription factor families in rice and *Arabidopsis*. BMC Genom. 13, 544.

Kim, J.Y., Seo, W.D., Park, D.-S., Jang, K.C., Choi, K.-J., Kim, S.-Y., Oh, S.-H., Ra, J.-E., Yi, G., Park, S.-K., Hwang, U.-H., Song, Y.-C., Park, B.-R., Park, M.-J., Kang, H.-W., Nam, M.-H., Han, S.-I., 2013. Comparative studies on major nutritional components of black waxy rice with giant embryos and its rice bran. Food Sci. Biotechnol. 22, 121–128.

Kim, S.R., Lee, D.Y., Yang, J.I., Moon, S., An, G., 2009. Cloning vectors for rice. J. Plant Biol. 52, 73–78.

Kim, T.J., Choi, J., Kim, K.W., Ahn, S.K., Ha, S.-H., Choi, Y., Park, N.I., Kim, J.K., 2017. Metabolite profiling of peppers of various colors reveals relationships between tocopherol, carotenoid, and phytosterol content. J. Food Sci. 82, 2885–2893.

Kim, T.J., Lee, K.B., Baek, S.-A., Choi, J., Ha, S.-H., Lim, S.-H., Park, S.-Y., Yeo, Y., Park, S.U., Kim, J.K., 2015. Determination of lipophilic metabolites for species discrimination and quality assessment of nine leafy vegetables. J. Kor. Soc. Appl. Biol. Chem. 58, 909–918.

Ko, M.R., Song, M.-H., Kim, J.K., Baek, S.-A., You, M.K., Lim, S.-H., Ha, S.-H., 2018. RNAi-mediated suppression of three carotenoid-cleavage dioxygenase genes, OsCCD1, 4a, and 4b, increases carotenoid content in rice. J. Exp. Bot. 69, 5105–5116.

Kopsell, D.A., Sams, C.E., 2013. Increases in shoot tissue pigments, glucosinolates, and mineral elements in sprouting broccoli after exposure to short-duration blue light from light emitting diodes. J. Am. Soc. Hortic. Sci. 138, 31–37.

Kutmon, M., van Iersel, M., Bohler, A., Kelder, T., Nunes, N., Pico, A.R., Evelo, C.T., 2015. PathVisio 3: an extendable pathway analysis toolbox. PLoS Comput. Biol. 11, e1004085.

Lau, O.S., Deng, X.W., 2012. The photomorphogenic repressors COP1 and DET1: 20 years later. Trends Plant Sci. 17, 584–593.

Lakshmanan, M., Lim, S.-H., Mohanty, B., Kim, J.K., Ha, S.-H., Lee, D., 2015. Unraveling the light-specific metabolic and regulatory signatures of rice through combined in silico modeling and multi-omics analysis. Plant Physiol. 169, 3002–3020.

Lee, Y.-M., Han, S.-I., Won, Y.-J., Lee, E., Park, E., Hwang, S.-Y., Yeum, K.-J., 2016. Black rice with giant embryo attenuates obesity-associated metabolic disorders in *ob/ob* mice. J. Agric. Food Chem. 64, 2492–2497.

Li, Q., Kubota, C., 2009. Effects of supplemental light quality on growth and phytochemicals of baby leaf lettuce. Environ. Exp. Bot. 67, 59–64.

Linde, A., Eklund, D.M., Kubota, A., Pederson, E.R.A., Holm, K., Gyllenstrand, N., Nishihama, R., Cronberg, N., Muranaka, T., Oyama, T., Kohchi, T., Lagercrantz, U., 2017. Early evolution of the land plant circadian clock. New Phytol. 216, 576–590.

Llorente, B., Martinez-Garcia, J.F., Stange, C., Rodriguez-Concepcion, M., 2017. Illuminating colors: regulation of carotenoid biosynthesis and accumulation by light. Curr. Opin. Plant Biol. 37, 49–55.

Lu, S.X., Knowles, S.M., Andronis, C., Ong, M.S., Tobin, E.M., 2009. Circadian clock associated1 and Late elongated hypocotyl function synergistically in the circadian clock of *Arabidopsis*. Plant Physiol. 150, 834–843.

Martín, G., Leivar, P., Ludevid, D., Tepperman, J.M., Quail, P.H., Monte, E., 2016. Phytochrome and retrograde signalling pathways converge to antagonistically regulate a light-induced transcriptional network. Nat. Commun. 7, 11431.

Mizoguchi, T., Wheatley, K., Hanzawa, Y., Wright, L., Mizoguchi, M., Song, H., Carré, I. A., Coupland, G., 2002. LHY and CCA1 are partially redundant genes required to maintain circadian rhythms in *Arabidopsis*. Dev. Cell 2, 629–641.

Nagel, D.H., Doherty, C.J., Pruneda-Paz, J.L., Schmitz, R.J., Ecker, J.R., Kay, S.A., 2015. Genome-wide identification of CCA1 targets uncovers an expanded clock network in *Arabidopsis*. Proc. Natl. Acad. Sci. Unit. States Am. 112, 4802–4810.

Nakamura, H., Muramatsu, M., Hakata, M., Ueno, O., Nagamura, Y., Hirochika, H., Takano, M., Ichikawa, H., 2009. Ectopic overexpression of the transcription factor OsGLK1 induces chloroplast development in non-green rice cells. Plant Cell Physiol. 50, 1933–1949.

Nascimento, L.B.S., Leal-Costa, M.V., Coutinho, M.A.S., Moreira, N.d.S., Lage, C.L.S., Barbi, N.d.S., Costa, S.S., Tavares, E.S., 2013. Increased antioxidant activity and changes in phenolic profile of *Kalanchoe pinnata* (Lamarck) Persoon (Crassulaceae) specimens grown under supplemental blue light. Photochem. Photobiol. 89, 391–399.

Nonaka, S., Arai, C., Takayama, M., Matsukura, C., Ezura, H., 2017. Efficient increase of ɣ-aminobutyric acid (GABA) content in tomato fruits by targeted mutagenesis. Sci. Rep. 7, 7057.

Ouzounis, T., Rosenqvist, E., Ottosen, C., 2015. Spectral effects of artificial light on plant physiology and secondary metabolism: a review. Hortscience 50, 1128–1135.

Paik, I., Huq, E., 2019. Plant photoreceptors: multi-functional sensory proteins and their signaling networks. Semin. Cell Dev. Biol. 92, 114–121.

Paine, J.A., Shipton, C.A., Chaggar, S., Howells, R.M., Kennedy, M.J., Vernon, G., Wright, S.Y., Hinchliffe, E., Adams, J.L., Silverstone, A.L., Drake, R., 2005. Improving the nutritional value of Golden Rice through increased pro-vitamin A content. Nat. Biotechnol. 23, 482–487.

Park, D.Y., Shim, Y., Gi, E., Lee, B.-D., An, G., Kang, K., Paek, N.-C., 2018. The MYB-related transcription factor RADIALIS-LIKE3 (OsRL3) functions in ABA-induced leaf senescence and salt sensitivity in rice. Environ. Exp. Bot. 156, 86–95.

Park, S.-H., Yi, N., Kim, Y.S., Jeong, M.-H., Bang, S.-W., Choi, Y.D., Kim, J.-K., 2010. Analysis of five novel putative constitutive gene promoters in transgenic rice plants. J. Exp. Bot. 61, 2459–2467.

Rawat, R., Schwartz, J., Jones, M.A., Sairanen, I., Cheng, Y., Andersson, C.R., Zhao, Y., Harmer, S.L., Kay, S.A., 2009. Reveille1, a Myb-like transcription factor, integrates the circadian clock and auxin pathways. Proc. Natl. Acad. Sci. Unit. States Am. 106, 16883–16888.

Rossini, L., Cribb, L., Martin, D.J., Langdale, J.A., 2001. The maize golden2 gene defines a novel class of transcriptional regulators in plant. Plant Cell 13, 1231–1244.

Sakuraba, Y., Kim, E.-Y., Han, S.-H., Piao, W., An, G., Todaka, D., Yamaguchi-Shinozaki, K., Paek, N.-C., 2017. Rice phytochrome-interacting factor-like1 (OsPIL1) is involved in the promotion of chlorophyll biosynthesis through feed-forward regulatory loops. J. Exp. Bot. 68, 4103–4114.

Shen, G., Hu, W., Zhang, B., Xing, Y., 2015. The regulatory network mediated by circadian clock genes is related to heterosis in rice. J. Integr. Plant Biol. 57, 300–312.

Smita, S., Katiyar, A., Chinnusamy, V., Pandey, D.M., Bansal, K.C., 2015. Transcriptional regulatory network analysis of MYB transcription factor family genes in rice. Front. Plant Sci. 6, 1157.

Song, Y., Jiang, Y., Kuai, B., Li, L., 2018. Circadian clock-associated 1 inhibits leaf senescence in *Arabidopsis*. Front. Plant Sci. 9, 280.
Sun, C., Zhang, K., Zhou, Y., Xiang, L., He, C., Zhong, C., Li, K., Wang, Q., Yang, C., Wang, Q., Chen, C., Chen, D., Wang, Y., Liu, C., Yang, B., Wu, H., Chen, X., Li, W., Wang, J., Xu, P., Wang, P., Fang, J., Chu, C., Deng, X., 2021. Dual function of clock component OsLHY sets critical day length for photoperiodic flowering in rice. Plant Biotechnol. J. 19, 1644–1657.
Tanaka, M., Takamura, T., Watanabe, H., Endo, M., Yanagi, T., Okamoto, K., 1998. *In vitro* growth of *Cymbidium* plantlets cultured under superbright red and blue light-emitting diodes (LEDs). J. Hortic. Sci. Biotechnol. 73, 39–44.
Tang, X., Miao, M., Niu, X., Zhang, D., Cao, X., Jin, X., Zhu, Y., Fan, Y., Wang, H., Liu, Y., Sui, Y., Wang, W., Wang, A., Xiao, F., Giovannoni, J., Liu, Y., 2016. Ubiquitin−conjugated degradation of golden 2−like transcription factor is mediated by CUL 4−DDB 1−based E 3 ligase complex in tomato. New Phytol. 209, 1028–1039.
Toledo-Ortiz, G., Johansson, H., Lee, K.P., Bou-Torrent, J., Stewart, K., Steel, G., Rodríguez-Concepción, M., Halliday, K.J., 2014. The HY5-PIF regulatory module coordinates light and temperature control of photosynthetic gene transcription. PLoS Genet. 10, e1004416.
Wang, F., Han, T., Song, Q., Ye, W., Song, X., Chu, J., Li, J., Chen, Z.J., 2020. The rice circadian clock regulates tiller growth and panicle development through strigolactone signaling and sugar sensing. Plant Cell 32, 3124–3138.
Waters, M.T., Langdale, J.A., 2009. The making of a chloroplast. EMBO J. 28, 2861–2873.
Waters, M.T., Wang, P., Korkaric, M., Capper, R.G., Saunders, N.J., Langdale, J.A., 2009. GLK transcription factors coordinate expression of the photosynthetic apparatus in *Arabidopsis*. Plant Cell 21, 1109–1128.
Xu, G., Guo, H., Zhang, D., Chen, D., Jiang, Z., Lin, R., 2015. REVEILLE1 promotes NADPH: protochlorophyllide oxidoreductase A expression and seedling greening in Arabidopsis. Photosynth. Res. 126, 331–340.
Yakir, E., Hilman, D., Hassidim, M., Green, R.M., 2007. CIRCADIAN CLOCK ASSOCIATED1 transcript stability and the entrainment of the circadian clock in Arabidopsis. Plant Physiol. 145, 925–932.
Yang, L., Jiang, Z., Jing, Y., Lin, R., 2020. PIF1 and RVE1 form a transcriptional feedback loop to control light-mediated seed germination in *Arabidopsis*. J. Integr. Plant Biol. 9, 1372–1384.
Ye, X., Al-Babili, S., Klöti, A., Zhang, J., Lucca, P., Beyer, P., Potrykus, I., 2000. Engineering the provitamin A (β-carotene) biosynthetic pathway into (carotenoid-free) rice endosperm. Science 287, 303–305.
You, M.K., Lee, Y.J., Kim, J.K., Baek, S.A., Jeon, Y.-A., Lim, S.-H., Ha, S.-H., 2020. The organ-specific differential roles of rice DXS and DXR, the first two enzymes of the MEP pathway, in carotenoid metabolism in *Oryza sativa* leaves and seeds. BMC Plant Biol. 20, 167.
Yuan, M., Zhao, Y., Zhang, Z., Chen, Y., Ding, C., Yuan, S., 2017. Light regulates transcription of chlorophyll biosynthetic genes during chloroplast biogenesis. Crit. Rev. Plant Sci. 36, 35–54.
Zhu, Q., Wang, B., Tan, J., Liu, T., Li, L., Liu, Y., 2020. Plant synthetic metabolic engineering for enhancing crop nutritional quality. Plant Commun. 1, 100017.

Overexpression of OsMYBR22/OsRVE1 Transcription Factor Simultaneously Enhances Chloroplast-dependent Metabolites in Rice Grains

Ye Sol Jeong[a,b,†], Heebak Choi[a,†], Jae Kwang Kim[c], Seung-A Baek[c], Min-Kyoung You[a], Dongho Lee[b], Sun-Hyung Lim[d,*], and Sun-Hwa Ha[a,*]

[a] *Department of Genetics and Biotechnology, College of Life Sciences, Kyung Hee University, Yongin, 17104, Republic of Korea*

[b] *Department of Biotechnology, College of Life Sciences and Biotechnology, Korea University, Seoul 02841, Republic of Korea*

[c] *Division of Life Sciences and Bio-Resource and Environmental Center, Incheon National University, Incheon 22012, Republic of Korea*

[d] *School of Biotechnology, Division of Horticultural Biotechnology, Hankyong National University, Anseong 17579, Republic of Korea*

* Authors for correspondence: Sun-Hyung Lim; Tel.: +82316705105; Email: limsh2@hknu.ac.kr; Sun-Hwa Ha; Tel.: +82312012654; Email: sunhwa@khu.ac.kr

† These authors contributed equally to this work.

Supplementary data

Table S1. List of primers used in this study

Table S2. Composition and contents of chlorophylls and carotenoids in the leaves of NT under white and blue light condition shown in Fig. 1.

Table S3. Composition and contents of chlorophylls and carotenoids in the leaves of NT and *OsMYBR22*-OX lines shown in Fig. 2.

Table S4. Composition and contents of chlorophylls and carotenoids in seeds at four developmental stages from NT and *OsMYBR22*-OX rice lines, which are shown in Fig. 3.

Table S5. Composition and contents of hydrophilic compounds in seeds at four developmental stages from NT and *OsMYBR22*-OX rice lines visualized in Fig. 5

Table S6. Composition and contents of lipophilic compounds in seeds at four developmental stages from NT and *OsMYBR22*-OX rice lines visualized in Fig. 5

Fig. S1. Subcellular localization of OsMYBR22 and generation of *OsMYBR22*-OX transgenic rice plants. (A) Schematic diagram of *GFP*-fused and *Myc*-tagged-*OsMYBR22* vector constructs. UBQ-P, maize ubiquitin promoter; *GFP*, green fluorescent protein gene; 35S-T, CaMV 35S terminator; PGD1-P, phosphogluconate dehydrogenase 1 constitutive promoter; *6xMyc*, 6 copies of the *Myc* tag repeats; Nos-T, nopaline synthase terminator; BAR, bialaphos resistance gene cassette. (B) Fluorescence observation by transfection of two GFP fusion vectors, *pOsMYBR22-sGFP* (in *pGA3452*) and *peGFP-OsMYBR22* (in *pGA3652*), in rice protoplasts. The nucleus was visualized by transfection of a NLS-conjugated RFP vector (in *pGA3574*). (C) Western blot analysis of *OsMYBR22*-OX transgenic lines using anti-Myc antibodies. Coomassie brilliant blue (CBB) staining represents the use of equal amounts of total protein. (D) TaqMan PCR analysis of

OsMYBR22-OX transgenic lines in the T0 generation using a *Bar* probe. (E) qRT-PCR analysis of *OsMYBR22*-OX transgenic lines using the *OsMYBR22* primer set. The same amounts of leaf RNA were normalized with *OsUBQ5* as an internal control; all reactions were performed in triplicate and the results were calculated by the ΔCt method against target genes, with error bars representing the standard deviations. NT, nontransgenic plant; PC, positive control of homozygotic plants with a single copy of expressed *Bar* T-DNA; C, C-terminal *Myc*-tagged *OsMYBR22*-OX line; N, N-terminal *Myc*-tagged *OsMYBR22*-OX line. All the primers used are listed in Table S1.

Fig. S2. Box plots displaying eight agronomic traits between NT and two representative *OsMYBR22*-OX lines. The rice plants were grown in a paddy field at Kyung Hee University in Yongin, South Korea (37° 24' N latitude, 127° 08' E longitude) during the summer until maturity. Yield parameters were scored for 30 individual plants per line with fully mature and dried grains after harvesting and threshing. The statistical significance was calculated via two-tailed Student's t-test (***, $p < 0.001$; **, $p < 0.01$; *, $p < 0.05$).

Fig. S3. Schematic representation of the regulatory relationships and metabolic pathways for chlorophylls and carotenoids. The metabolites are denoted in regular black, the regulatory TF genes used in this study are shown in bold blue with gray boxes, and the pathway genes are shown in *italicized* black (not used in this study) or blue (used in this study). The black solid arrow indicates a single enzymatic step and the black dotted arrow represents multiple enzymatic steps in a metabolic pathway. The red pointed arrows and blue blunted lines indicate transcriptionally positive and negative regulation, respectively. The red solid line represents the physical interaction between proteins that act synergistically. The abbreviations of genes in *italicized* black are as follows: *CAO*, chlorophyllide a oxygenase gene; *CHLG*,

chlorophyll synthase gene; *CHLP*, geranylgeranyl diphosphate reductase gene; *CrtISO*, carotenoid isomerase gene; *DVR*, divinyl chlorophyllide *a* 8-vinyl-reductase gene; *HCAR*, hydroxymethyl chlorophyll *a* reductase gene; *Lhca* and *Lhcb*, light-harvesting Chl a/b-binding protein a and b genes; *NCED*, 9-*cis*-epoxycarotenoid dioxygenase gene; *PPH*, pheophytinase gene; *RBCS*, ribulose bisphosphate carboxylase small subunit gene; *ZDS*, ζ-carotene desaturase gene; *ZEP*, zeaxanthin epoxidase gene; *ZISO*, ζ-carotene isomerase gene. See the abbreviations for the rest of the genes in the legend of Fig. 4.

Fig. S4. Expression levels of chlorophylls and carotenoid metabolism-related genes between NT and two *OsMYBR22*-OX lines using qRT-PCR; the same genes were used for the heat map displays in Fig. 4. Original bar (A) and line (B) graphs showing the expression of four CCA1-like subfamily and nine chlorophyll biosynthesis-associated genes in flag leaves at 150 days after germination (DAG) and in the seeds at 30, 40, 50 and 60 days after flowering (DAF) during development, respectively. Original bar (C) and line (D) graphs showing eleven chlorophyll degradation-associated gene expressions in the leaves and seeds at the same stages. Original bar graphs showing 16 carotenoid biosynthetic pathway gene expression levels in leaves at 150 DAG (E) and seeds at 60 DAF (F). The statistical significance was calculated via two-tailed Student's t-test (***, $p < 0.001$; **, $p < 0.01$; *, $p < 0.05$). Information on the gene ID and PCR primer sets is listed in Table S1. The abbreviations of the genes are the same as those in the legend of Fig. 4.

Table S1. List of primers used in this study.

Experiment	Gene (MSU ID)	Primer set	Primer sequence (5'-3')
Cloning			
Localization	OsMYBR22 (Os02g46030)	OsMYBR22-pGA3652(N)_F/	GTGTTAACGGATCCGGTACCATGGAGATGGCCTGTTTGCC/
		OsMYBR22-pGA3652(N)_R	GGAAATTCGAGCTCGGTACCTCACAAGCACAGCCTTGTCAGC
		OsMYBR22-pGA3452(C)_F/	TTACTTCTGCAGCCCGGGATGGAGATGGCCTGTTTGC/
		OsMYBR22-pGA3452(C)_R	CCATTCTAGAACTAGTCAAGCACAGCCTTGTCAGC
Overexpression	OsMYBR22 (Os02g46030)	OsMYBR22-OE_CF/	AAAAAAGCAGGCTTTATGGAGATGGCCTGTTTGCC/
		OsMYBR22-OE_CR	TGAATTGGTTCCTTTCCCAAGCACAGCCTTGTCAGCTCACCGTCGGCG
		OsMYBR22-OE_NF/	TTGAATTCCGGAAGCCCGATGGAGATGGCCTGTTTGCCGGGAAAC/
		OsMYBR22-OE_NR	ATCTGTACCGGATCCCTCACAAGCACAGCCTTGTC
qRT-PCR			
OsMYBR22	OsMYBR22 (Os02g46030)	Transgene_QF/	CGGAGAGCGAGCTGCTGCGATCGG/
		Transgene_QR	GTTTGAACGATCGGGGAAATTCC
		Endogenous_QF/	CCTCATCAACAACATCGAGGAGA/
		Endogenous_QR	CCTATGTGCTCTTGTATACGGC
		Total_QF/	GTTTGCCGGGAAACGCCATG/
		Total_QR	CGTAGTTCATATGGCTCCTGAGA
Chlorophyll biosynthesis-associated gene	OsRVE1 (Os02g46030)	Total_QF/	GTTTGCCGGGAAACGCCATG/
		Total_QR	CGTAGTTCATATGGCTCCTGAGA
	OsRVE2 (Os04g49450)	OsRVE2_QF/	CAAATGACGAGGAGGTCAAGG/
		OsRVE2_QR	CAGGGGCTGACATCTGATGT
	OsRVE3 (Os06g51260)	OsRVE3_QF/	CAGTCCCACAAGGAAATAGACCA/
		OsRVE3_QR	CTTCCTTGGATCTGGGATGAC
	OsCCA1 (Os08g06110)	OsCCA1_QF/	GGAAGTTTCTGAAGAGGGTCGT/
		OsCCA1_QR	GCATTCTTGTTGAGGTCAACCGT
	OsGLK1 (Os06g24070)	OsGLK1_QF/	CCATGCCAGCTGCGAGATTTC/
		OsGLK1_QR	GCGTCGATGCTCTCGCTTGATG
	OsGLK2 (Os01g13740)	OsGLK2_QF/	TTGATGCCCACCCGTCTAAGG/
		OsGLK2_QR	GTGCAGCTCAGACATGACGC
	OsHY5 (Os06g39960)	OsHY5_QF/	GCCTCAAAAGATTGCTGAGGAAC/
		OsHY5_QR	TTCAGCACCTGCCTAAGCATC
	OsPIL1 (Os03g56950)	OsPIL1_QF/	GTGCCACCACAGGTATCAGGA/
		OsPIL1_QR	TCCATCAGAGGTTGGTGGTTG
	OsHEMA1 (Os10g35840)	OsHEMA1_QF/	TTCAAGATCTCCGCCGACCGG/
		OsHEMA1_QR	GACTGGTGAGTTCTGAGATAGCACG
	OsCHLH (Os03g20700)	OsCHLH_QF/	GGCAGAGCTGAAGAGGAAAACTAAGG/
		OsCHLH_QR	CTCGATGAGGGCCTCAGCTGTG
	OsChl27 (Os01g17170)	OsChl27_QF/	GAGACCAACCGCACAACAGCAAGG/
		OsChl27_QR	ATATCGTCAGACTCGCCTATGG
	OsPorA (Os04g58200)	OsPorA_QF/	CTTGTTCCGCGAGCACATCC/
		OsPorA_QR	TTCCAGCTCCAGTACACGCC
	OsPorB (Os10g35370)	OsPorB_QF/	CATCACCGGGAACACGAACACGC/
		OsPorB_QR	TGTCCTTGTAGGCCTTGGCG
Chlorophyll degradation-associated gene	OsDET1 (Os01g01484)	OsDET1_QF/	TGGTAGTGTGGATGGAGGGG/
		OsDET1_QR	CGATGAATTTTGTGGATTTGTGT
	OsFLU1 (Os01g32730)	OsFLU1_QF/	TTGGGTGATCACGTCGAAGA/
		OsFLU1_QR	TTCTGTAACACCTGCGTCCT
	OsFLU2 (Os02g37470)	OsFLU2_QF/	CCCAGGAAGCAACAACTGAC/
		OsFLU2_QR	TCAAAGCGATCTCCTACGCT
	OsORE1 (Os02g36880)	OsORE1_QF/	AGGAGCTCATCACGCACTACC/
		OsORE1_QR	TCGGGTACTTCCGGTCCTTCA
	OsRL3 (Os02g47744)	OsRL3_QF/	TGAAAGTTGTGGTACCTCCTCCT/
		OsRL3_QR	AAGGACGTGGATCGCATTGAC
	OsNYC1 (Os01g12710)	OsNYC1_QF/	ATGAAGAGGGAAGAGCAGTATA/
		OsNYC1_QR	GAGCGAGAACACAGAAACCCATG
	OsNOL (Os03g45194)	OsNOL_QF/	CCTATAATTCCTTCTACTCGCAGC/
		OsNOL_QR	GGCGAGCCAGTTGATGACG
	OsCLH (Os10g28370)	OsCLH_QF/	TACCCGGTGGTGGTGTTCTTG/
		OsCLH_QR	GTGGTATCCGGTCCAGACAT
	OsSGR (Os09g36200)	OsSGR_QF/	AGGGGTGGTACAACAAGCTG/
		OsSGR_QR	GCTCCTTGCGGAAGATGTAG
	OsPaO (Os03g05310)	OsPaO_QF/	CAAGGGCTGCTCTTCGTGTG/
		OsPaO_QR	TCATAGCCATAGTACAGATCCC
	OsRCCR1 (Os10g25030)	OsRCCR1_QF/	CCAGTCCTCACTACACTGCAA/
		OsRCCR1_QR	CCAGAAGCACCACGATCGAA
Carotenoid biosynthetic gene	OsDXS1 (Os05g33840)	OsDXS1_QF/	GAGATCAGTGAATTGTATATTAGTCGGCG/
		OsDXS1_QR	CGGGTCTCCGTCCACGAACAACTGAAGAGC
	OsDXS2 (Os07g09190)	OsDXS2_QF/	GGGGGAGGTTCCAGTAAGAA/
		OsDXS2_QR	TCATTTTGCATTTGGAAGCA
	OsDXS3 (Os06g05100)	OsDXS3_QF/	GCTGTTTCATGGATATTCTTCAGTCTTTC/
		OsDXS3_QR	CCTTCCTGTTACAAGCACTTGATAGGG
	OsDXR (Os01g01710)	OsDXR_QF/	GCTCCATGCATAGTCAGCAG/
		OsDXR_QR	GCACGGACGAACGATTTATT
	OsPSY1 (Os06g51290)	OsPSY1_QF/	GGGAAGATGATGAGCAGGTTA/
		OsPSY1_QR	GCATTTTCCCTATACATGCT
	OsPSY2 (Os12g43130)	OsPSY2_QF/	TGTATGCCATAAGCCTGCCAC/
		OsPSY2_QR	TATGCTTCTTGAACTGTGGGG
	OsPSY3 (Os09g38320)	OsPSY3_QF/	TGTAAGATGGGTATGTACCCC/
		OsPSY3_QR	TGAGCTCATGCTAATGATCCT
	OsPDS (Os03g08570)	OsPDS_QF/	TGTGTCATCATCCCCTAGTCA/
		OsPDS_QR	TCAGCTCTCAGTCACAAATC
	OsLCYE (Os01g39960)	OsLCYE_QF/	GTATGGCAGCGTTCACAGGGAC/
		OsLCYE_QR	GCCAGCGTCATAGCATCGTCTC
	OsCYP97A4 (Os02g57290)	OsCYP97A4_QF/	AAGTCTCAGCAACTCGAATCTGAGTTATG/
		OsCYP97A4_QR	TGTAGCGCGAATCACCAAGATAAGCCTG
	OsCYP97B4 (Os02g07680)	OsCYP97B4_QF/	ATCATCCACCAGTTGGCACCAAAAGCTGT/
		OsCYP97B4_QR	CTTACCCTTGTATTGGTTGTTGTCTGC
	OsCYP97C2 (Os10g39930)	OsCYP97C2_QF/	CAATGGCCTGTATATGAATGTAAGTCTG/
		OsCYP97C2_QR	TCAACCTGTACGCCGATATTTACCACAT
	OsLCYB (Os02g09750)	OsLCYB_QF/	CGTCCAGTACGACAAGCCGTA/
		OsLCYB_QR	AAGGGCATGGCGTAGAGGAACG
	OsBCH1 (Os03g03370)	OsBCH1_QF/	TCGAGAACGTGCCCTACTTCC/
		OsBCH1_QR	ACCCACCTCCTCCAACTCCTT
	OsBCH2 (Os04g48880)	OsBCH2_QF/	AGAGCTGGAGAAGGAGCTTGC/
		OsBCH2_QR	AAAAATCTTGCAAGGCAAAGG
	OsBCH3 (Os10g38940)	OsBCH3_QF/	TCAAGAAGAGGATCAAGAGGA/
		OsBCH3_QR	AGGAAAAGCCAAAACAAAAGCG
Internal reference	OsUBQ5 (Os01g22490)	OsUBQ5_QF/	GAAGTAAGGAAGGAGGAGGA/
		OsUBQ5_QR	AAGGTGTTCAGTTCCAAGG

Table S2. Composition and contents of chlorophylls and carotenoids in the leaves of NT under white and blue light condition shown in Fig. 1.

Compound	Light condition		Fold change
	White	Blue	Blue/White
Chlorophyll content (μg/mg)			
Chlorophyll *a*	0.68 ± 0.06	1.00 ± 0.11	1.47
Chlorophyll *b*	0.23 ± 0.03	0.29 ± 0.03	1.26
Total chlorophyll	**0.91 ± 0.08**	**1.29 ± 0.14**	**1.42**
Carotenoid content (μg/g)			
α-Carotene	0.85 ± 0.07	0.98 ± 0.12	1.15
β-Carotene	65.53 ± 3.79	84.18 ± 11.95	1.28
Lutein	33.43 ± 2.77	39.95 ± 5.81	1.20
Zeaxanthin	0.64 ± 0.07	2.34 ± 0.38	3.66
Violaxanthin	1.47 ± 0.13	1.92 ± 0.29	1.31
Total carotenoid	**101.93 ± 6.79**	**129.37 ± 18.54**	**1.27**
β/α ratio	1.97	2.16	

The chlorophyll contents were expressed as the sum of chlorophyll *a* and *b*. The total carotenoid contents were calculated as the sum of the five carotenoid components, and the *β*-carotene content was expressed as the sum of *E-β*-carotene, *9Z-β*-carotene and *13Z-β*-carotene. All the data are expressed as the means (micrograms per milligram and micrograms per gram of fresh weight for chlorophyll and carotenoids, respectively) ± standard errors of three independent experiments using leaves at 150 d after germination that were simultaneously grown in the same field conditions for all materials. The *β/α* in terms of carotenoid contents is the ratio of *β,β*-carotenoids such as *β*-carotene, zeaxanthin and violaxanthin relative to *β,ε*-carotenoids such as *ε*-carotene and lutein.

Table S3. Composition and contents of chlorophylls and carotenoids in the leaves of NT and *OsMYBR22*-OX lines shown in Fig. 2

Compound	Plant		
	NT	C8	N11
Chlorophyll content (μg/mg)			
Chlorophyll *a*	0.82 ± 0.02	1.26 ± 0.01	1.47 ± 0.01
Chlorophyll *b*	0.29 ± 0.00	0.41 ± 0.00	0.48 ± 0.00
Total chlorophyll	1.12 ± 0.03	1.68 ± 0.02	1.95 ± 0.02
Carotenoid content (μg/g)			
α-Carotene	2.00 ± 0.06	6.98 ± 0.98	9.61 ± 0.37
β-Carotene	177.07 ± 1.64	341.27 ± 34.78	346.57 ± 18.60
Lutein	100.53 ± 2.63	133.13 ± 12.42	154.19 ± 11.95
Zeaxanthin	26.26 ± 0.39	9.58 ± 0.77	14.03 ± 1.05
Violaxanthin	4.55 ± 0.13	5.51 ± 0.77	6.30 ± 0.7
Total carotenoids	310.42 ± 4.68	496.48 ± 49.66	530.72 ± 32.04
β/α ratio	2.03	2.54	2.24

Chlorophyll content was expressed as the sum of chlorophylls *a* and *b*. The total carotenoid content was calculated as the sum of the five carotenoid components and the *β*-carotene content was expressed as the sum of *E-β*-carotene, *9Z-β*-carotene, and *13Z-β*-carotene. All the data are expressed as the means (micrograms per milligram and micrograms per gram of fresh weight for chlorophyll and carotenoids, respectively) ± standard errors of three independent experiments using leaves at 150 days after germination that were simultaneously grown in the same field conditions for all materials. The *β/α* in terms of carotenoid content is the ratio of *β,β*-carotenoids such as *β*-carotene, zeaxanthin, and violaxanthin relative to *β,ε*-carotenoids such as *ε*-carotene and lutein.

Table S4. Composition and content of chlorophylls and carotenoids in seeds at four developmental stages from NT and *OsMYBR22*-OX rice lines, which are shown in Figs. 3 and 5

Group	Compound	DAF	30			40			50			60		
		Plant	NT	C8	N11	NT	C8	N11	NT	C8	N11	NT	C8	N11
1	**Chlorophyll (μg/mg)**													
	Chlorophyll *a*		0.01 ± 0.00	0.04 ± 0.00	0.05 ± 0.00	0.00 ± 0.00	0.04 ± 0.00	0.05 ± 0.00	0.00 ± 0.00	0.02 ± 0.00	0.02 ± 0.00	0.00 ± 0.00	0.02 ± 0.00	0.04 ± 0.00
	Chlorophyll *b*		0.00 ± 0.00	0.02 ± 0.00	0.02 ± 0.00	0.00 ± 0.00	0.01 ± 0.00	0.02 ± 0.00	0.00 ± 0.00	0.01 ± 0.00	0.01 ± 0.00	0.00 ± 0.00	0.01 ± 0.00	0.01 ± 0.00
	Total chlorophyll		0.01 ± 0.00	0.06 ± 0.00	0.07 ± 0.00	0.00 ± 0.00	0.05 ± 0.00	0.07 ± 0.00	0.01 ± 0.00	0.03 ± 0.00	0.03 ± 0.00	0.00 ± 0.00	0.04 ± 0.00	0.05 ± 0.00
2	**Carotenoids (μg/g)**													
	α-Carotene		0.00 ± 0.00	0.11 ± 0.00	0.14 ± 0.00	0.00 ± 0.00	0.09 ± 0.00	0.11 ± 0.01	0.00 ± 0.00	0.04 ± 0.00	0.07 ± 0.01	0.00 ± 0.00	0.04 ± 0.00	0.08 ± 0.01
	β-Carotene		0.90 ± 0.05	5.42 ± 0.17	8.34 ± 0.32	0.16 ± 0.00	4.79 ± 0.18	6.56 ± 0.11	0.11 ± 0.00	2.75 ± 0.25	4.90 ± 0.15	0.04 ± 0.00	1.96 ± 0.05	4.32 ± 0.09
	Lutein		0.98 ± 0.04	5.30 ± 0.17	7.19 ± 0.12	0.36 ± 0.00	5.40 ± 0.24	6.49 ± 0.21	0.26 ± 0.00	4.08 ± 0.45	5.53 ± 0.22	0.14 ± 0.01	3.64 ± 0.10	5.41 ± 0.09
	Zeaxanthin		0.15 ± 0.01	0.13 ± 0.01	0.31 ± 0.01	0.05 ± 0.00	0.14 ± 0.01	0.28 ± 0.01	0.08 ± 0.00	0.46 ± 0.06	0.54 ± 0.02	0.04 ± 0.00	0.45 ± 0.02	0.56 ± 0.01
	Violaxanthin		0.00 ± 0.00	0.19 ± 0.00	0.37 ± 0.02	0.00 ± 0.00	0.17 ± 0.01	0.25 ± 0.02	0.00 ± 0.00	0.10 ± 0.01	0.19 ± 0.01	0.00 ± 0.00	0.08 ± 0.01	0.16 ± 0.01
	Total carotenoids		2.03 ± 0.10	11.15 ± 0.36	16.34 ± 0.45	0.57 ± 0.00	10.58 ± 0.43	13.69 ± 0.35	0.45 ± 0.01	7.42 ± 0.77	11.23 ± 0.41	0.22 ± 0.01	6.17 ± 0.14	10.54 ± 0.14
	β/α ratio		1.07	1.06	1.23	0.58	0.93	1.07	0.73	0.80	1.01	0.57	0.68	0.92

The chlorophyll contents were expressed as the sum of chlorophylls *a* and *b*. The total carotenoid content was calculated as the sum contents of the five carotenoid components and the *β*-carotene content was expressed as the sum of *E-β*-carotene, *9Z-β*-carotene, and *13Z-β*-carotene. All the data are expressed as the means (micrograms per milligram and micrograms per gram of fresh weight for chlorophyll and carotenoids, respectively) ± standard errors of three independent experiments using rice seeds at 30, 40, 50, and 60 days after flowering that were simultaneously grown and harvested under the same field conditions for all materials. The *β/α* in terms of carotenoid contents is the ratio of *β,β*-carotenoids such as *β*-carotene, zeaxanthin, and violaxanthin relative to *β,ε*-carotenoids such as *ε*-carotene and lutein.

Table S5. Composition and content of hydrophilic compounds in seeds at four developmental stages from NT and *OsMYBR22*-OX rice lines visualized in Fig. 5

Group	Compound	DAF	30			40			50			60		
		Plant	NT	C8	N11	NT	C8	N11	NT	C8	N11	NT	C8	N11
3	**Sugars (ratio/g)**													
	Starch		49.73 ± 8.23	49.75 ± 3.23	51.45 ± 3.76	48.33 ± 3.54	54.40 ± 4.12	50.10 ± 1.57	56.45 ± 2.20	57.17 ± 1.01	51.00 ± 2.43	55.32 ± 3.67	49.11 ± 1.99	46.33 ± 3.68
	Arabinose		0.58 ± 0.01	1.19 ± 0.01	0.94 ± 0.01	0.15 ± 0.00	1.29 ± 0.03	1.61 ± 0.06	0.12 ± 0.01	0.84 ± 0.01	1.05 ± 0.01	0.10 ± 0.00	0.85 ± 0.04	1.10 ± 0.02
	Fructose		40.40 ± 1.75	189.28 ± 4.48	440.67 ± 4.88	6.92 ± 0.79	126.03 ± 2.71	241.77 ± 1.37	6.53 ± 0.13	74.21 ± 2.82	180.58 ± 2.20	5.66 ± 0.48	66.64 ± 5.74	130.64 ± 6.39
	Fructose-6-phosphate		0.04 ± 0.02	0.39 ± 0.13	1.25 ± 0.14	0.09 ± 0.03	0.18 ± 0.02	0.44 ± 0.11	0.05 ± 0.02	0.06 ± 0.01	0.32 ± 0.06	0.05 ± 0.02	0.05 ± 0.01	0.24 ± 0.05
	Galactose		2.24 ± 0.12	2.53 ± 0.33	2.85 ± 0.18	0.75 ± 0.07	3.24 ± 0.20	3.63 ± 0.09	0.69 ± 0.07	2.59 ± 0.17	3.32 ± 0.42	0.61 ± 0.10	3.09 ± 0.20	3.57 ± 0.26
	Glucose		30.68 ± 1.63	82.19 ± 5.55	123.56 ± 2.42	3.48 ± 0.25	61.19 ± 4.05	72.38 ± 5.76	2.94 ± 0.13	41.21 ± 1.30	68.83 ± 5.60	2.63 ± 0.02	32.47 ± 2.01	52.99 ± 1.93
	Glucose-6-phosphate		0.08 ± 0.03	1.24 ± 0.46	4.17 ± 0.54	0.27 ± 0.09	0.52 ± 0.07	1.31 ± 0.39	0.14 ± 0.06	0.17 ± 0.01	0.96 ± 0.26	0.12 ± 0.04	0.14 ± 0.01	0.67 ± 0.18
	Glyceric acid		0.64 ± 0.06	1.86 ± 0.44	3.41 ± 0.11	0.24 ± 0.11	1.43 ± 0.06	2.36 ± 0.14	0.12 ± 0.04	0.86 ± 0.01	1.73 ± 0.09	0.13 ± 0.01	0.99 ± 0.01	1.86 ± 0.07
	Glycerol		5.25 ± 0.23	14.41 ± 1.50	18.99 ± 0.47	2.09 ± 0.13	11.88 ± 0.53	17.90 ± 0.62	2.09 ± 0.14	8.35 ± 0.23	12.35 ± 0.46	1.83 ± 0.18	7.22 ± 0.14	10.72 ± 0.35
	Inositol		4.52 ± 0.03	20.03 ± 0.46	24.26 ± 0.25	1.36 ± 0.08	15.69 ± 0.40	22.05 ± 0.28	1.26 ± 0.08	6.89 ± 0.08	15.06 ± 0.21	1.36 ± 0.12	6.30 ± 0.21	13.04 ± 0.51
	Mannitol		0.08 ± 0.01	0.15 ± 0.01	0.14 ± 0.01	0.07 ± 0.01	0.21 ± 0.01	0.24 ± 0.01	0.24 ± 0.01	0.24 ± 0.01	0.20 ± 0.01	0.13 ± 0.01	0.73 ± 0.01	0.43 ± 0.02
	Mannose		0.37 ± 0.03	1.68 ± 0.16	2.93 ± 0.03	0.00 ± 0.00	1.21 ± 0.05	2.50 ± 0.15	0.00 ± 0.00	0.51 ± 0.03	1.43 ± 0.04	0.00 ± 0.00	0.26 ± 0.04	0.85 ± 0.02
	Raffinose		4.82 ± 1.06	2.47 ± 0.14	2.13 ± 0.02	4.45 ± 0.75	3.40 ± 0.27	3.56 ± 0.23	6.65 ± 1.19	4.15 ± 0.31	4.40 ± 0.29	5.27 ± 0.20	5.97 ± 0.46	5.75 ± 0.40
	Sucrose		142.98 ± 10.06	106.49 ± 5.69	130.77 ± 8.37	170.75 ± 18.93	134.86 ± 10.41	161.83 ± 14.85	217.63 ± 30.31	161.66 ± 10.46	163.97 ± 12.29	214.46 ± 9.58	211.49 ± 9.09	173.08 ± 6.61
	Threonic acid		0.11 ± 0.01	0.26 ± 0.01	0.48 ± 0.03	0.06 ± 0.01	0.25 ± 0.01	0.53 ± 0.02	0.05 ± 0.01	0.13 ± 0.01	0.23 ± 0.01	0.00 ± 0.00	0.21 ± 0.00	0.34 ± 0.01
	Xylose		0.20 ± 0.03	0.35 ± 0.03	0.49 ± 0.01	0.00 ± 0.00	0.24 ± 0.02	0.42 ± 0.03	0.00 ± 0.00	0.19 ± 0.01	0.24 ± 0.01	0.00 ± 0.00	0.20 ± 0.01	0.27 ± 0.01
4	**Organic acids (ratio/g)**													
	Citric acid		1.09 ± 0.30	0.82 ± 0.22	2.85 ± 0.21	0.68 ± 0.20	1.49 ± 0.35	1.81 ± 0.34	0.84 ± 0.20	1.23 ± 0.26	1.63 ± 0.32	0.80 ± 0.07	1.26 ± 0.20	1.80 ± 0.31
	Fumaric acid		0.25 ± 0.07	1.53 ± 0.70	3.96 ± 0.07	0.24 ± 0.08	1.26 ± 0.19	2.83 ± 0.52	0.22 ± 0.07	0.57 ± 0.04	2.03 ± 0.28	0.21 ± 0.07	0.59 ± 0.03	2.16 ± 0.32
	Lactic acid		0.93 ± 0.12	0.76 ± 0.09	0.73 ± 0.10	0.77 ± 0.07	0.85 ± 0.07	0.66 ± 0.10	0.72 ± 0.05	1.01 ± 0.11	0.79 ± 0.07	1.01 ± 0.12	0.99 ± 0.18	1.03 ± 0.14
	Malic acid		1.73 ± 0.47	11.49 ± 3.30	34.93 ± 0.98	1.44 ± 0.44	10.30 ± 2.09	23.20 ± 5.04	1.35 ± 0.51	5.47 ± 0.84	15.73 ± 2.75	1.21 ± 0.42	6.15 ± 0.77	18.89 ± 3.31
	Pyruvic acid		0.10 ± 0.03	0.14 ± 0.03	0.17 ± 0.01	0.02 ± 0.00	0.12 ± 0.03	0.12 ± 0.03	0.01 ± 0.00	0.07 ± 0.01	0.13 ± 0.02	0.01 ± 0.00	0.05 ± 0.00	0.11 ± 0.02
	Quinic acid		0.05 ± 0.02	0.09 ± 0.01	0.20 ± 0.00	0.03 ± 0.02	0.08 ± 0.01	0.14 ± 0.01	0.01 ± 0.01	0.05 ± 0.01	0.12 ± 0.00	0.01 ± 0.00	0.05 ± 0.00	0.12 ± 0.01
	Succinic acid		3.23 ± 1.04	4.71 ± 0.99	7.31 ± 0.47	2.34 ± 1.65	4.04 ± 1.12	7.67 ± 0.41	1.77 ± 1.04	2.84 ± 0.73	4.73 ± 0.45	1.35 ± 0.82	1.91 ± 0.60	3.52 ± 0.34

5	**Aromatic acid and aromatic amico acid (ratio/g)**												
	Ferulic acid	0.03 ± 0.00	0.05 ± 0.00	0.04 ± 0.00	0.04 ± 0.01	0.05 ± 0.01	0.05 ± 0.01	0.03 ± 0.01	0.04 ± 0.01	0.05 ± 0.01	0.03 ± 0.01	0.05 ± 0.01	0.05 ± 0.00
	Shikimic acid	0.11 ± 0.04	0.12 ± 0.04	0.06 ± 0.02	0.10 ± 0.05	0.11 ± 0.03	0.12 ± 0.05	0.08 ± 0.04	0.09 ± 0.03	0.09 ± 0.03	0.08 ± 0.03	0.10 ± 0.03	0.08 ± 0.03
	Sinapinic acid	0.01 ± 0.00	0.01 ± 0.00	0.02 ± 0.00	0.01 ± 0.00	0.02 ± 0.00	0.02 ± 0.00	0.01 ± 0.00	0.02 ± 0.00	0.03 ± 0.00	0.02 ± 0.00	0.02 ± 0.00	0.02 ± 0.00
	Phenylalanine	0.29 ± 0.02	0.92 ± 0.08	1.25 ± 0.07	0.24 ± 0.12	1.04 ± 0.04	1.57 ± 0.11	0.22 ± 0.04	0.81 ± 0.04	1.32 ± 0.15	0.21 ± 0.04	0.79 ± 0.04	1.29 ± 0.10
	Tryptophan	0.20 ± 0.04	0.54 ± 0.09	0.68 ± 0.08	0.30 ± 0.05	0.55 ± 0.04	0.79 ± 0.07	0.36 ± 0.05	0.49 ± 0.04	0.77 ± 0.14	0.33 ± 0.04	0.51 ± 0.04	0.71 ± 0.06
	Tyrosine	0.64 ± 0.05	1.65 ± 0.20	2.79 ± 0.21	0.58 ± 0.21	1.93 ± 0.08	3.15 ± 0.21	0.62 ± 0.13	1.78 ± 0.09	3.07 ± 0.33	0.61 ± 0.13	1.87 ± 0.09	2.73 ± 0.21
6	**Amino acids (ratio/g)**												
	Alanine	4.31 ± 0.43	8.98 ± 0.78	24.13 ± 2.96	5.61 ± 2.24	12.75 ± 1.66	27.65 ± 2.23	6.59 ± 0.37	10.81 ± 1.00	13.94 ± 3.18	7.65 ± 0.98	10.06 ± 0.85	14.93 ± 0.76
	Asparagine	0.82 ± 0.20	2.46 ± 0.69	1.30 ± 0.19	1.23 ± 0.38	4.59 ± 1.33	2.11 ± 0.51	1.13 ± 0.37	3.86 ± 1.17	2.01 ± 0.55	1.23 ± 0.25	4.32 ± 1.26	3.86 ± 1.12
	Aspartic acid	1.42 ± 0.28	5.23 ± 1.19	7.85 ± 0.91	1.66 ± 0.13	6.87 ± 1.13	7.60 ± 0.98	1.88 ± 0.05	7.83 ± 1.11	8.15 ± 1.76	1.88 ± 0.34	8.55 ± 0.73	10.24 ± 0.74
	Cysteine	0.03 ± 0.01	0.06 ± 0.00	0.19 ± 0.04	0.03 ± 0.01	0.08 ± 0.00	0.12 ± 0.01	0.04 ± 0.00	0.07 ± 0.00	0.08 ± 0.02	0.04 ± 0.01	0.07 ± 0.00	0.11 ± 0.02
	Glutamic acid	0.82 ± 0.12	1.13 ± 0.19	2.78 ± 0.10	1.15 ± 0.15	1.87 ± 0.27	5.11 ± 0.91	1.59 ± 0.22	1.62 ± 0.29	2.57 ± 0.56	1.98 ± 0.22	1.73 ± 0.25	2.03 ± 0.31
	Glutamine	0.23 ± 0.10	0.88 ± 0.36	0.83 ± 0.36	0.14 ± 0.05	1.84 ± 0.63	1.42 ± 0.49	0.19 ± 0.05	1.70 ± 0.72	0.95 ± 0.60	0.23 ± 0.08	1.79 ± 0.66	1.46 ± 0.48
	Glycine	0.94 ± 0.21	3.18 ± 1.39	6.27 ± 1.15	0.40 ± 0.02	3.15 ± 0.22	6.00 ± 0.50	0.93 ± 0.09	2.37 ± 0.15	4.30 ± 0.28	1.05 ± 0.02	2.30 ± 0.11	4.37 ± 0.23
	Isoleucine	0.64 ± 0.02	1.86 ± 0.37	2.47 ± 0.54	0.48 ± 0.16	1.89 ± 0.08	3.38 ± 0.21	0.44 ± 0.04	1.56 ± 0.11	2.67 ± 0.59	0.36 ± 0.00	1.43 ± 0.15	2.89 ± 0.28
	Leucine	1.13 ± 0.02	3.44 ± 0.76	4.49 ± 1.11	0.75 ± 0.31	3.62 ± 0.18	6.23 ± 0.46	0.56 ± 0.02	2.79 ± 0.23	4.84 ± 1.37	0.51 ± 0.01	2.51 ± 0.29	4.75 ± 0.55
	Lysine	0.19 ± 0.01	0.89 ± 0.10	1.54 ± 0.24	0.11 ± 0.03	0.88 ± 0.06	1.78 ± 0.16	0.14 ± 0.03	0.66 ± 0.05	1.32 ± 0.24	0.13 ± 0.03	0.61 ± 0.04	1.18 ± 0.08
	Methionine	0.18 ± 0.01	0.58 ± 0.07	0.87 ± 0.11	0.12 ± 0.06	0.56 ± 0.02	0.86 ± 0.08	0.11 ± 0.02	0.44 ± 0.03	0.74 ± 0.14	0.10 ± 0.02	0.33 ± 0.02	0.61 ± 0.05
	Proline	2.01 ± 0.09	3.50 ± 0.66	4.32 ± 1.30	2.34 ± 0.30	4.25 ± 0.15	6.32 ± 0.26	2.41 ± 0.22	4.04 ± 0.28	4.20 ± 1.35	2.82 ± 0.14	4.70 ± 0.39	5.44 ± 0.59
	Serine	0.51 ± 0.05	1.64 ± 0.18	3.65 ± 1.04	0.44 ± 0.14	1.99 ± 0.13	2.68 ± 0.27	0.44 ± 0.03	1.75 ± 0.14	3.74 ± 1.56	0.51 ± 0.05	2.06 ± 0.12	2.61 ± 0.22
	Threonine	0.39 ± 0.02	1.13 ± 0.08	1.54 ± 0.34	0.30 ± 0.12	1.17 ± 0.02	2.00 ± 0.09	0.29 ± 0.01	0.92 ± 0.04	1.44 ± 0.36	0.27 ± 0.01	0.99 ± 0.03	2.19 ± 0.13
	Valine	2.00 ± 0.05	5.32 ± 0.17	5.67 ± 1.06	1.31 ± 0.37	5.23 ± 0.18	6.99 ± 0.32	1.24 ± 0.08	4.74 ± 0.31	5.46 ± 1.12	2.65 ± 0.17	4.41 ± 0.33	5.67 ± 0.48
7	**Amino acid derivatives (ratio/g)**												
	β-Alanine	0.11 ± 0.02	0.24 ± 0.04	0.53 ± 0.13	0.12 ± 0.00	0.31 ± 0.04	0.49 ± 0.07	0.14 ± 0.01	0.25 ± 0.03	0.30 ± 0.01	0.16 ± 0.01	0.24 ± 0.02	0.38 ± 0.02
	Ethanolamine	2.60 ± 0.58	6.55 ± 0.69	9.61 ± 1.80	1.56 ± 0.05	7.10 ± 0.24	10.59 ± 0.40	1.27 ± 0.13	5.36 ± 0.16	7.05 ± 0.87	1.46 ± 0.07	6.02 ± 0.04	8.90 ± 0.15
	GABA	11.06 ± 2.42	33.28 ± 4.71	54.39 ± 10.22	6.73 ± 0.08	33.20 ± 2.96	42.44 ± 3.53	1.82 ± 0.18	28.88 ± 2.26	39.54 ± 6.03	4.30 ± 0.20	32.51 ± 2.58	48.66 ± 3.26
	Putrescine	0.03 ± 0.01	0.16 ± 0.01	0.59 ± 0.09	0.00 ± 0.00	0.13 ± 0.00	0.41 ± 0.01	0.00 ± 0.00	0.08 ± 0.00	0.17 ± 0.03	0.00 ± 0.00	0.08 ± 0.00	0.19 ± 0.00
	Pyroglutamic acid	2.61 ± 0.16	4.78 ± 0.29	4.82 ± 0.50	3.10 ± 0.90	7.65 ± 0.15	7.78 ± 0.66	3.60 ± 0.97	6.90 ± 0.39	6.18 ± 0.70	3.27 ± 0.74	7.19 ± 0.74	6.48 ± 0.59

The data are expressed as the means (ratio per gram of fresh weight) ± standard errors of three independent experiments using rice seeds at 30, 40, 50, and 60 days after flowering that were simultaneously grown and harvested in the same field condition for all materials.

Table S6. Composition and contents of lipophilic compounds in seeds at four developmental stages from NT and *OsMYBR22*-OX rice lines visualized in Fig. 5

Group	Compound	DAF	30			40			50			60		
		Plant	NT	C8	N11	NT	C8	N11	NT	C8	N11	NT	C8	N11
8	**Tocols (μg/g)**													
	α-Tocopherol		11.47 ± 0.90	13.52 ± 0.19	14.45 ± 0.42	13.56 ± 0.23	15.32 ± 0.88	13.31 ± 0.55	14.41 ± 2.34	12.77 ± 1.47	14.66 ± 0.64	14.37 ± 0.29	11.03 ± 0.21	13.52 ± 0.50
	β-Tocopherol		1.26 ± 0.04	1.58 ± 0.09	2.55 ± 0.11	1.30 ± 0.03	1.64 ± 0.06	2.76 ± 0.08	1.20 ± 0.04	1.45 ± 0.04	2.75 ± 0.03	1.17 ± 0.08	1.45 ± 0.03	2.37 ± 0.06
	γ-Tocopherol		1.94 ± 0.11	2.02 ± 0.10	2.32 ± 0.01	2.08 ± 0.06	1.99 ± 0.01	1.91 ± 0.08	1.65 ± 0.08	2.02 ± 0.14	1.97 ± 0.04	1.78 ± 0.06	1.66 ± 0.10	1.76 ± 0.14
	α-Tocotrienol		6.92 ± 0.41	6.21 ± 0.27	5.33 ± 0.13	7.77 ± 0.14	6.74 ± 0.24	5.73 ± 0.16	8.39 ± 0.79	5.87 ± 0.58	5.95 ± 0.29	8.46 ± 0.19	5.72 ± 0.15	5.65 ± 0.12
	γ-Tocotrienol		5.93 ± 0.14	5.27 ± 0.15	5.60 ± 0.24	5.17 ± 0.03	5.14 ± 0.18	5.53 ± 0.06	5.62 ± 0.37	4.27 ± 0.42	5.45 ± 0.15	5.37 ± 0.09	3.75 ± 0.06	4.49 ± 0.24
9	**Phytosterols (μg/g)**													
	Campesterol		184.64 ± 3.16	176.48 ± 11.62	153.05 ± 3.93	196.23 ± 3.15	181.07 ± 8.62	173.35 ± 5.13	195.37 ± 16.58	188.91 ± 9.87	173.30 ± 10.00	205.92 ± 12.00	201.63 ± 18.11	172.32 ± 7.31
	Cholesterol		3.48 ± 0.30	2.62 ± 0.27	2.68 ± 0.20	1.82 ± 0.09	2.00 ± 0.14	1.90 ± 0.04	2.03 ± 0.17	1.94 ± 0.01	2.04 ± 0.06	1.85 ± 0.32	1.85 ± 0.04	1.98 ± 0.18
	β-Sitosterol		193.07 ± 5.12	205.12 ± 11.17	181.80 ± 5.79	186.14 ± 3.79	207.77 ± 6.32	203.01 ± 6.41	198.99 ± 18.24	216.84 ± 11.49	201.33 ± 7.45	211.25 ± 9.85	238.96 ± 14.26	195.62 ± 2.11
	Stigmasterol		92.63 ± 2.50	96.65 ± 6.56	92.66 ± 6.13	91.90 ± 3.31	99.06 ± 3.34	95.56 ± 2.80	95.32 ± 6.11	94.12 ± 9.76	95.14 ± 3.75	99.01 ± 2.95	104.44 ± 7.91	91.40 ± 2.40
10	**Policosanols (μg/g)**													
	Eicosanol (C20)		1.83 ± 0.10	1.58 ± 0.03	1.64 ± 0.04	1.55 ± 0.01	1.47 ± 0.04	1.39 ± 0.05	1.63 ± 0.02	1.54 ± 0.04	1.52 ± 0.03	1.46 ± 0.08	1.47 ± 0.05	1.52 ± 0.08
	Heneicosanol (C21)		1.02 ± 0.03	0.83 ± 0.11	0.94 ± 0.06	0.86 ± 0.06	0.96 ± 0.08	0.86 ± 0.02	1.04 ± 0.07	1.00 ± 0.07	0.94 ± 0.06	0.91 ± 0.08	0.93 ± 0.04	0.91 ± 0.01
	Docosanol (C22)		5.91 ± 0.23	4.96 ± 0.19	4.97 ± 0.18	4.89 ± 0.15	4.92 ± 0.10	4.34 ± 0.04	6.30 ± 0.63	5.12 ± 0.33	4.75 ± 0.14	5.17 ± 0.65	5.19 ± 0.26	4.79 ± 0.37
	Tricosanol (C23)		0.40 ± 0.06	0.44 ± 0.07	0.39 ± 0.03	0.39 ± 0.06	0.38 ± 0.08	0.45 ± 0.04	0.48 ± 0.06	0.43 ± 0.08	0.47 ± 0.03	0.49 ± 0.07	0.43 ± 0.02	0.45 ± 0.05
	Tetracosanol (C24)		9.71 ± 0.05	9.57 ± 0.91	8.79 ± 0.20	6.54 ± 0.58	9.73 ± 0.21	9.91 ± 0.15	13.41 ± 1.23	11.95 ± 1.42	8.75 ± 0.44	14.90 ± 0.76	11.36 ± 1.25	9.84 ± 0.32
	Hexacosanol (C26)		14.98 ± 2.87	18.84 ± 1.43	15.61 ± 1.45	17.04 ± 0.78	12.11 ± 1.35	20.56 ± 3.54	23.47 ± 4.54	21.97 ± 3.33	14.13 ± 2.27	24.23 ± 3.08	22.60 ± 4.44	16.66 ± 2.30
	Heptacosanol (C27)		1.66 ± 0.01	1.67 ± 0.07	1.87 ± 0.11	1.98 ± 0.08	1.87 ± 0.03	1.78 ± 0.18	1.96 ± 0.12	2.01 ± 0.10	1.87 ± 0.01	2.04 ± 0.06	1.83 ± 0.18	2.01 ± 0.04
	Octacosanol (C28)		29.29 ± 4.51	34.91 ± 8.31	30.53 ± 1.59	23.37 ± 2.64	26.30 ± 2.75	29.85 ± 2.44	27.33 ± 1.80	24.37 ± 5.58	33.24 ± 5.49	34.27 ± 5.70	35.93 ± 5.32	30.07 ± 4.15
	Triacontanol (C30)		96.20 ± 19.93	138.60 ± 18.26	107.96 ± 4.16	69.36 ± 4.92	103.68 ± 8.91	136.64 ± 39.84	110.71 ± 28.59	106.68 ± 17.03	153.32 ± 22.67	92.97 ± 4.20	178.85 ± 67.96	133.84 ± 22.27

The data are expressed as the means (micrograms per gram of fresh weight) ± standard errors of three independent experiments using rice seeds at 30, 40, 50, and 60 days after flowering that were simultaneously grown and harvested under the same field conditions for all materials.

Fig. S1.

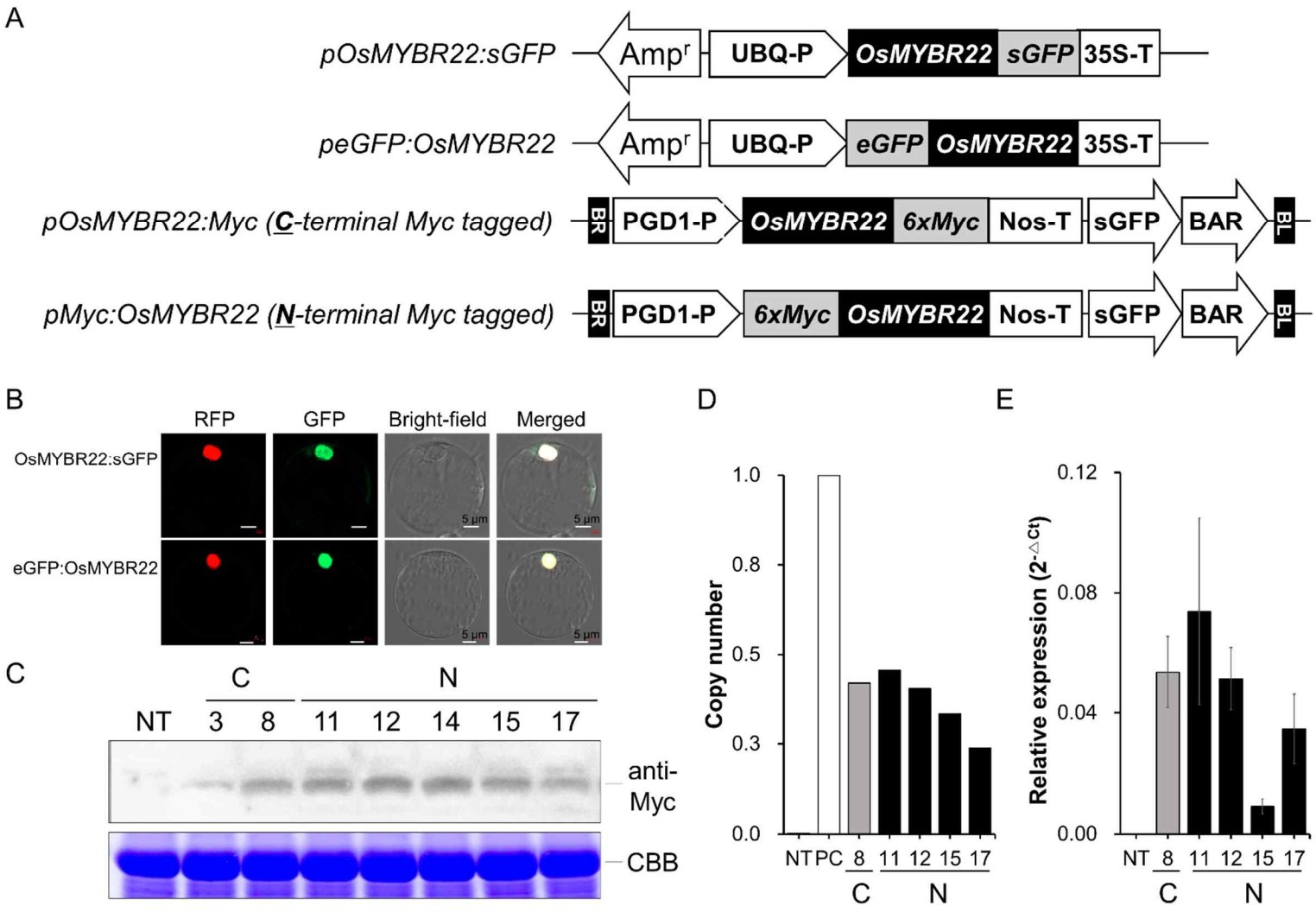
A
pOsMYBR22:sGFP
Amp^r
UBQ-P
OsMYBR22
sGFP
35S-T
peGFP:OsMYBR22
Amp^r
UBQ-P
eGFP
OsMYBR22
35S-T
pOsMYBR22:Myc (C-terminal Myc tagged)
BR
PGD1-P
OsMYBR22
6xMyc
Nos-T
sGFP
BAR
BL
pMyc:OsMYBR22 (N-terminal Myc tagged)
BR
PGD1-P
6xMyc
OsMYBR22
Nos-T
sGFP
BAR
BL
B
RFP
GFP
Bright-field
Merged
OsMYBR22:sGFP
eGFP:OsMYBR22
5 μm
C
C
N
NT
3
8
11
12
14
15
17
anti-Myc
CBB
D
Copy number
1.0
0.8
0.5
0.3
0.0
NT
PC
8
11
12
15
17
C
N
E
Relative expression (2^-△Ct)
0.12
0.08
0.04
0.00
NT
8
11
12
15
17
C
N

Fig. S2.

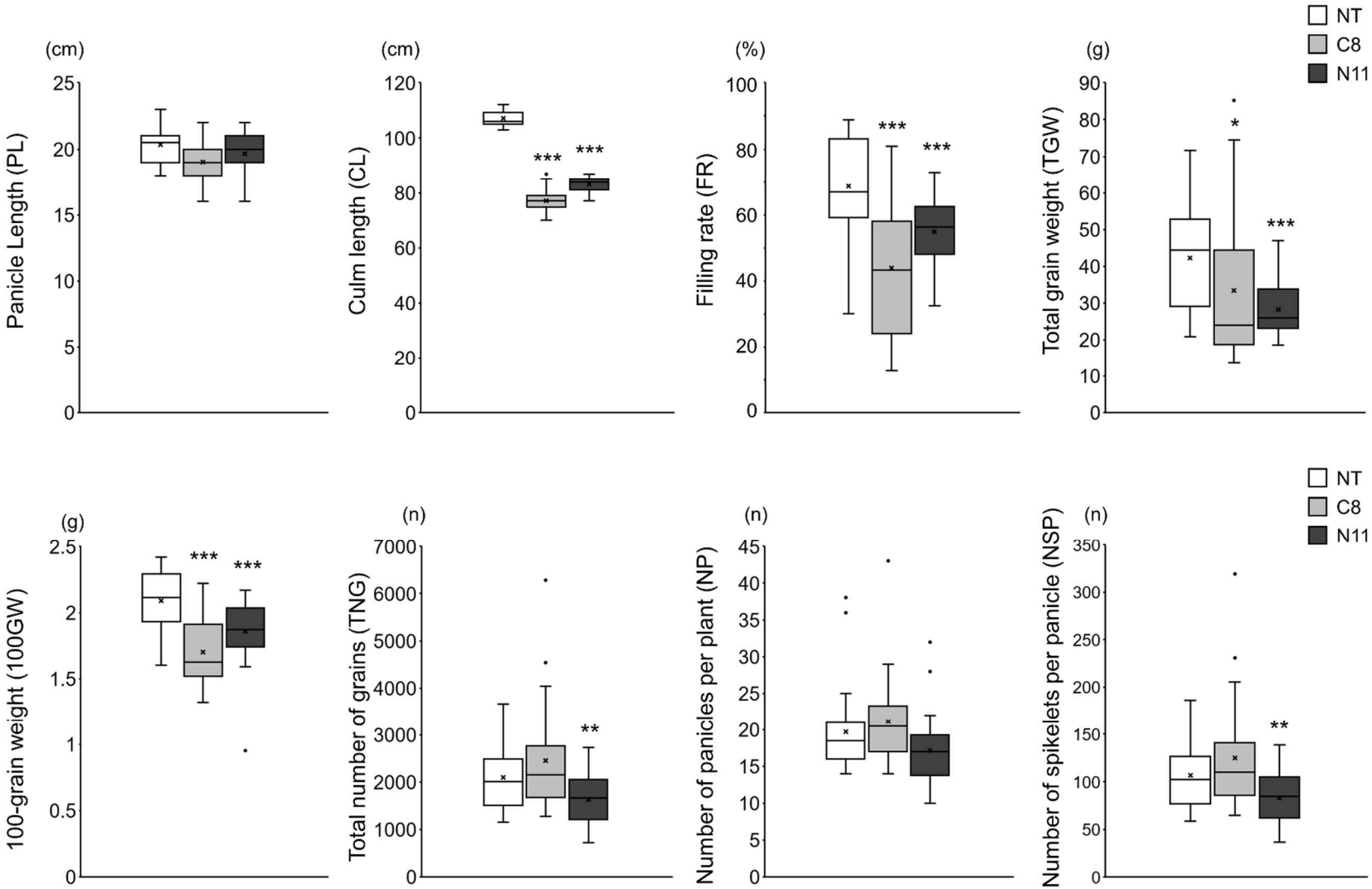
NT
C8
N11
(cm)
Panicle Length (PL)
(cm)
Culm length (CL)
(%)
Filling rate (FR)
(g)
Total grain weight (TGW)
(g)
100-grain weight (100GW)
(n)
Total number of grains (TNG)
(n)
Number of panicles per plant (NP)
(n)
Number of spikelets per panicle (NSP)

Fig. S3.

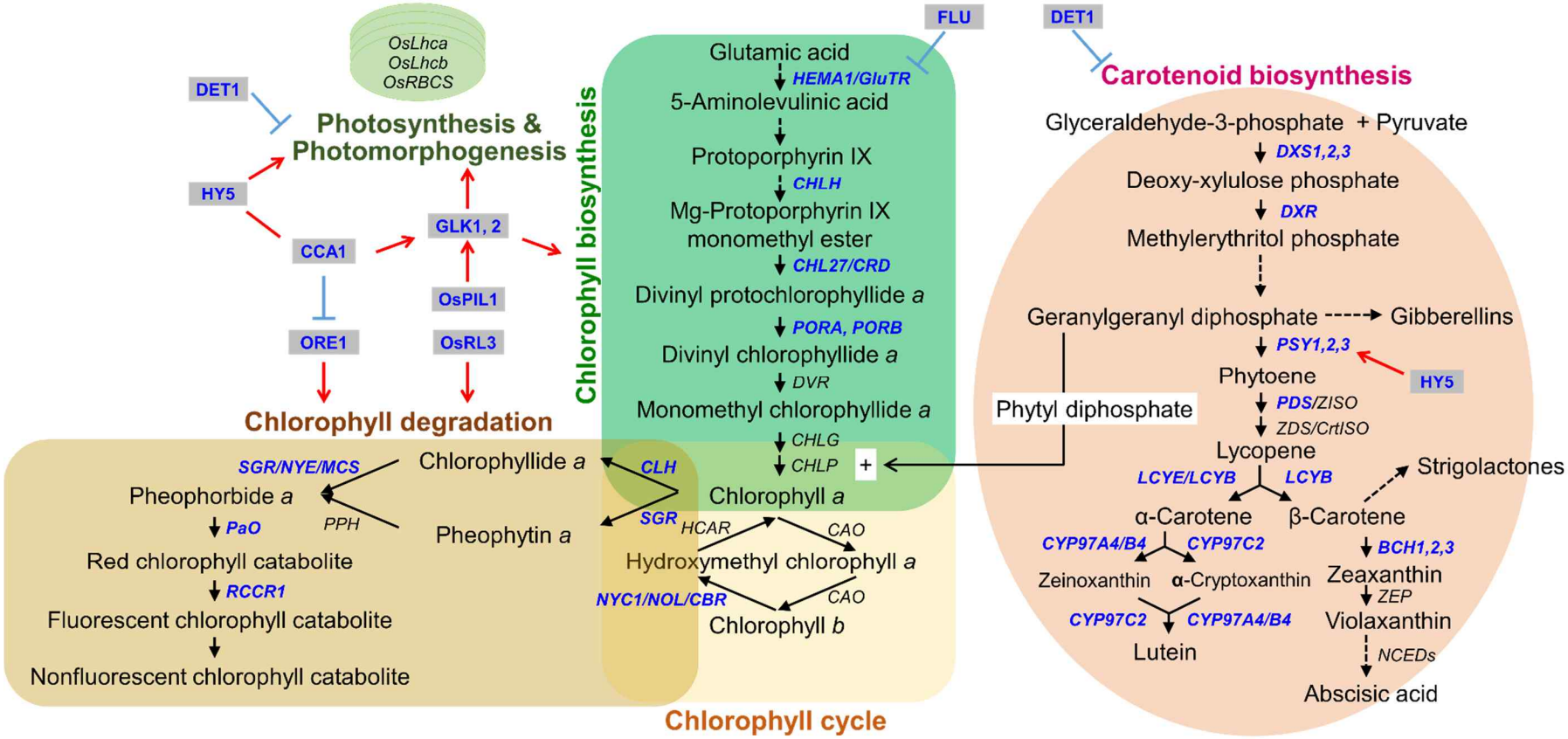
OsLhca
OsLhcb
OsRBCS
DET1
Photosynthesis &
Photomorphogenesis
HY5
CCA1
GLK1, 2
OsPIL1
ORE1
OsRL3
Chlorophyll degradation
SGR/NYE/MCS
Chlorophyllide a
Pheophorbide a
PaO
PPH
Pheophytin a
Red chlorophyll catabolite
RCCR1
Fluorescent chlorophyll catabolite
Nonfluorescent chlorophyll catabolite
Chlorophyll biosynthesis
FLU
Glutamic acid
HEMA1/GluTR
5-Aminolevulinic acid
Protoporphyrin IX
CHLH
Mg-Protoporphyrin IX
monomethyl ester
CHL27/CRD
Divinyl protochlorophyllide a
PORA, PORB
Divinyl chlorophyllide a
DVR
Monomethyl chlorophyllide a
CHLG
CHLP
+
CLH
Chlorophyll a
SGR
HCAR
CAO
Hydroxymethyl chlorophyll a
NYC1/NOL/CBR
CAO
Chlorophyll b
Chlorophyll cycle
DET1
Carotenoid biosynthesis
Glyceraldehyde-3-phosphate + Pyruvate
DXS1,2,3
Deoxy-xylulose phosphate
DXR
Methylerythritol phosphate
Geranylgeranyl diphosphate
Gibberellins
PSY1,2,3
Phytoene
HY5
Phytyl diphosphate
PDS/ZISO
ZDS/CrtISO
Lycopene
LCYE/LCYB
LCYB
Strigolactones
α-Carotene
β-Carotene
CYP97A4/B4
CYP97C2
BCH1,2,3
Zeinoxanthin
α-Cryptoxanthin
Zeaxanthin
ZEP
CYP97C2
CYP97A4/B4
Violaxanthin
Lutein
NCEDs
Abscisic acid

Fig. S4.

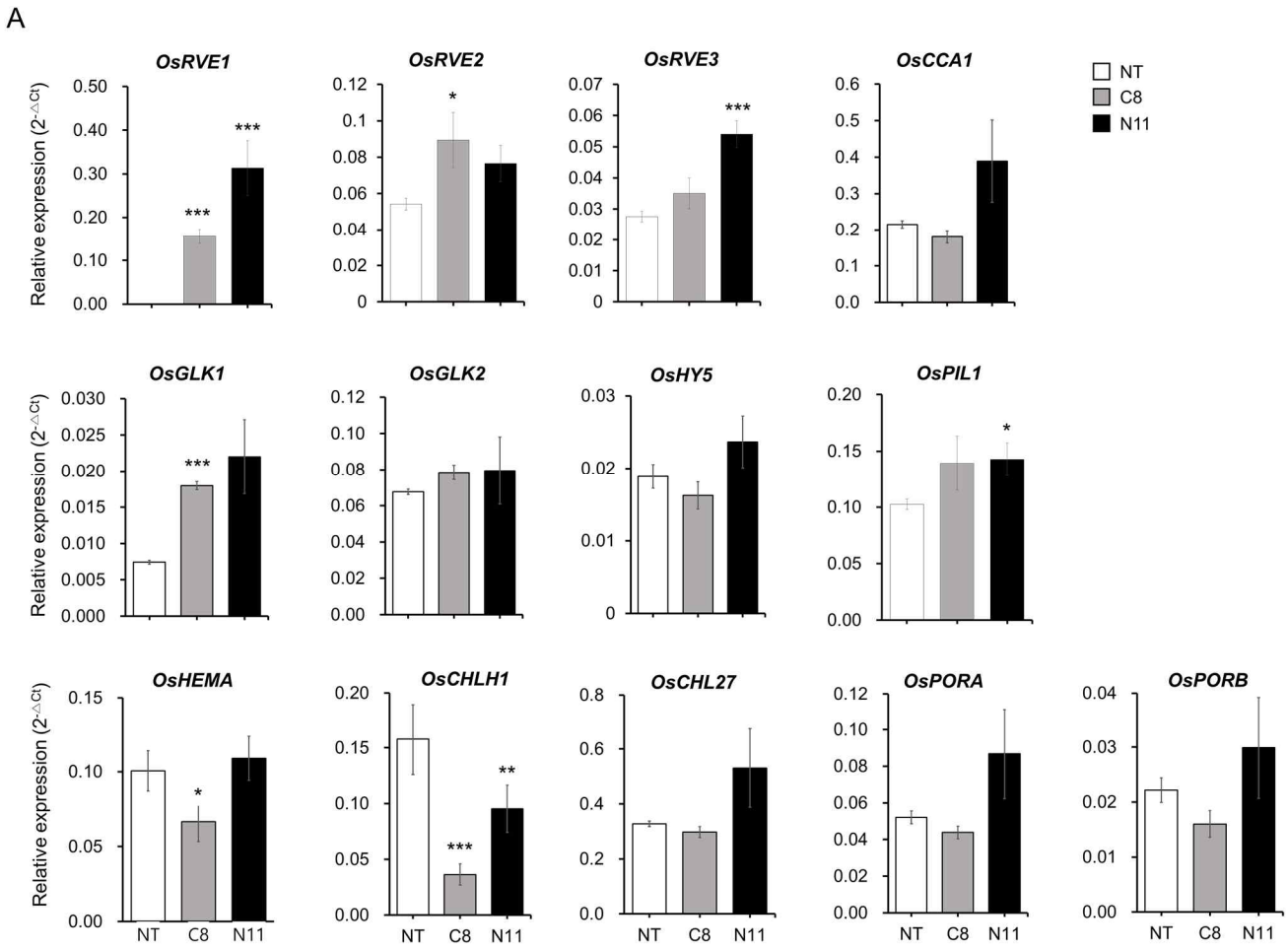
A
OsRVE1
OsRVE2
OsRVE3
OsCCA1
OsGLK1
OsGLK2
OsHY5
OsPIL1
OsHEMA
OsCHLH1
OsCHL27
OsPORA
OsPORB
Relative expression (2-△Ct)
NT
C8
N11

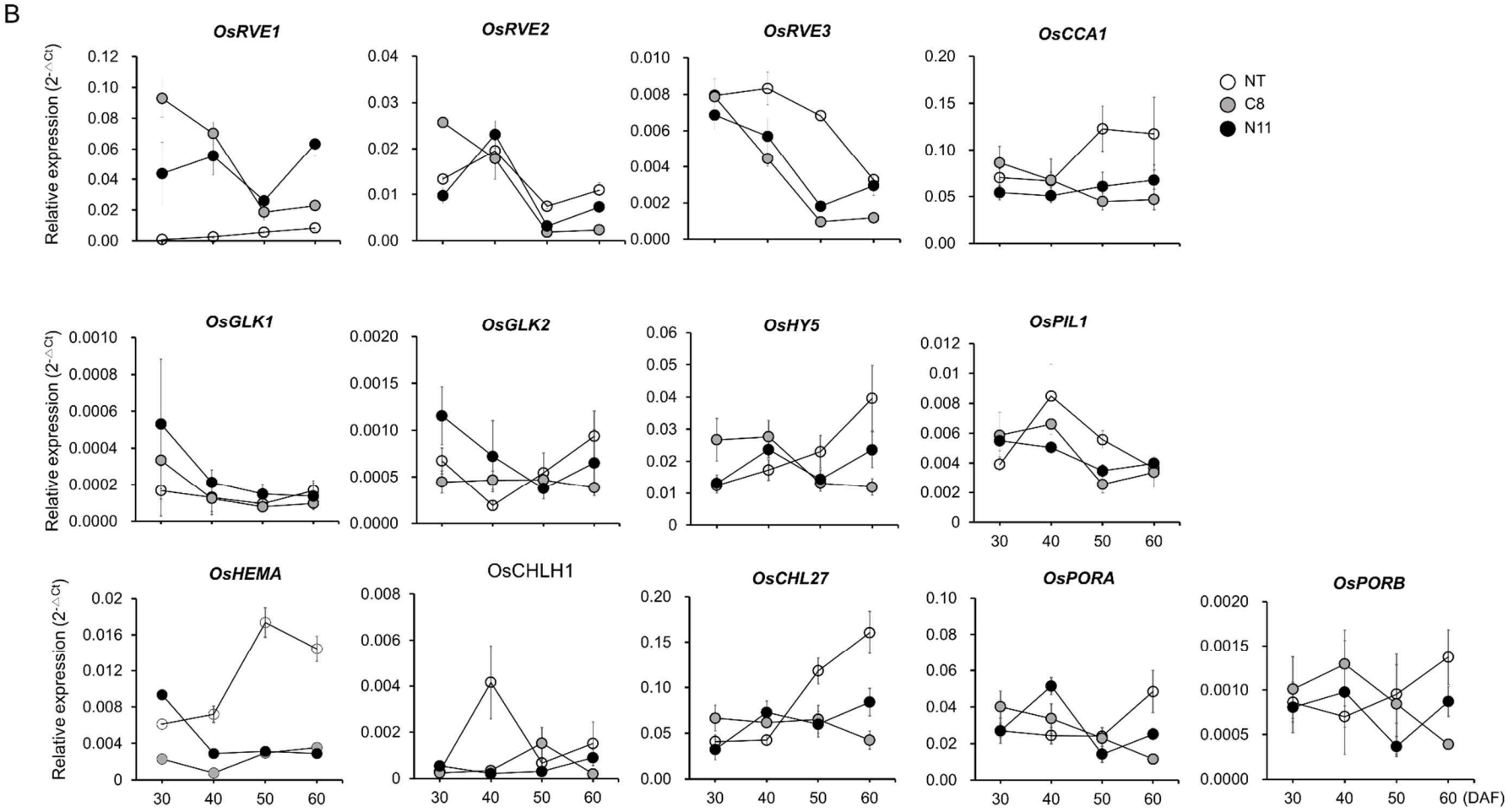
B
OsRVE1
OsRVE2
OsRVE3
OsCCA1
OsGLK1
OsGLK2
OsHY5
OsPIL1
OsHEMA
OsCHLH1
OsCHL27
OsPORA
OsPORB
Relative expression (2-△Ct)
NT
C8
N11
30
40
50
60
60 (DAF)

C

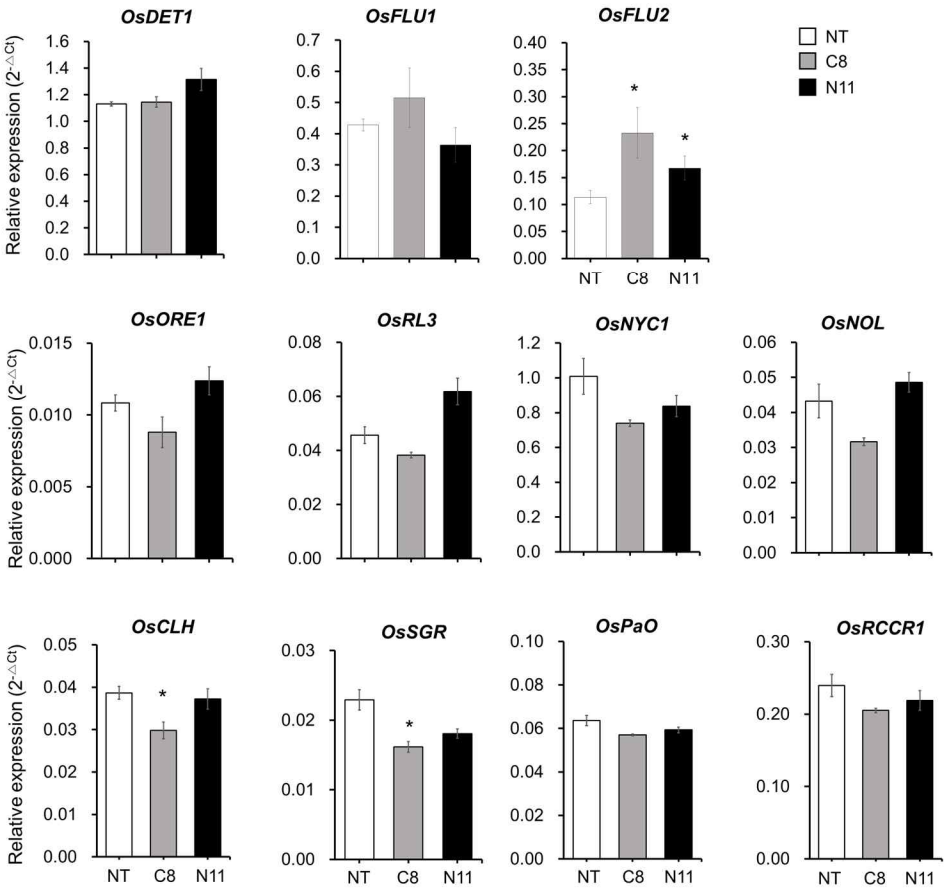
OsDET1
OsFLU1
OsFLU2
NT
C8
N11
Relative expression (2-△Ct)
OsORE1
OsRL3
OsNYC1
OsNOL
OsCLH
OsSGR
OsPaO
OsRCCR1

D

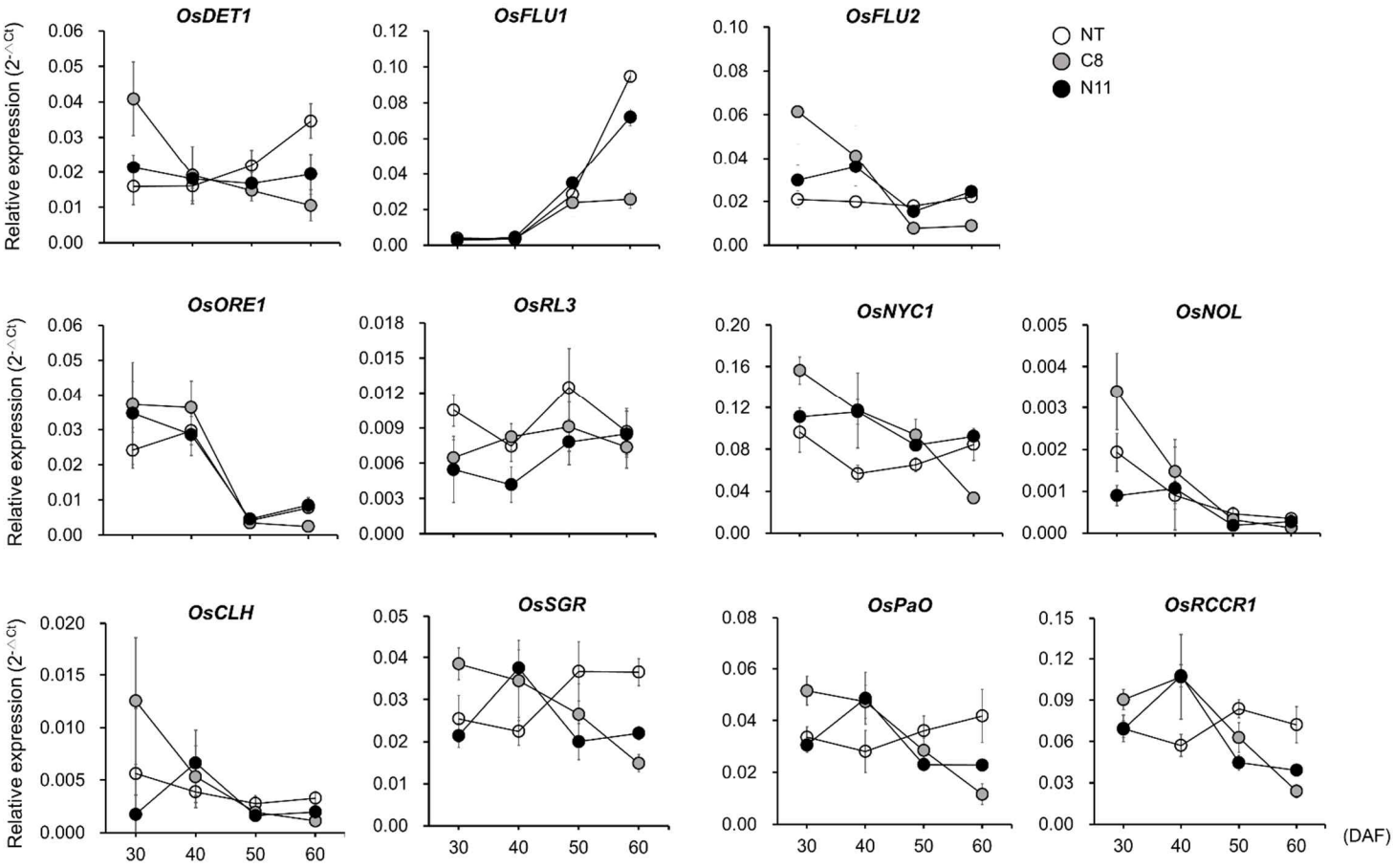
OsDET1
OsFLU1
OsFLU2
NT
C8
N11
Relative expression (2-ΔCt)
OsORE1
OsRL3
OsNYC1
OsNOL
OsCLH
OsSGR
OsPaO
OsRCCR1
30
40
50
60
(DAF)

E

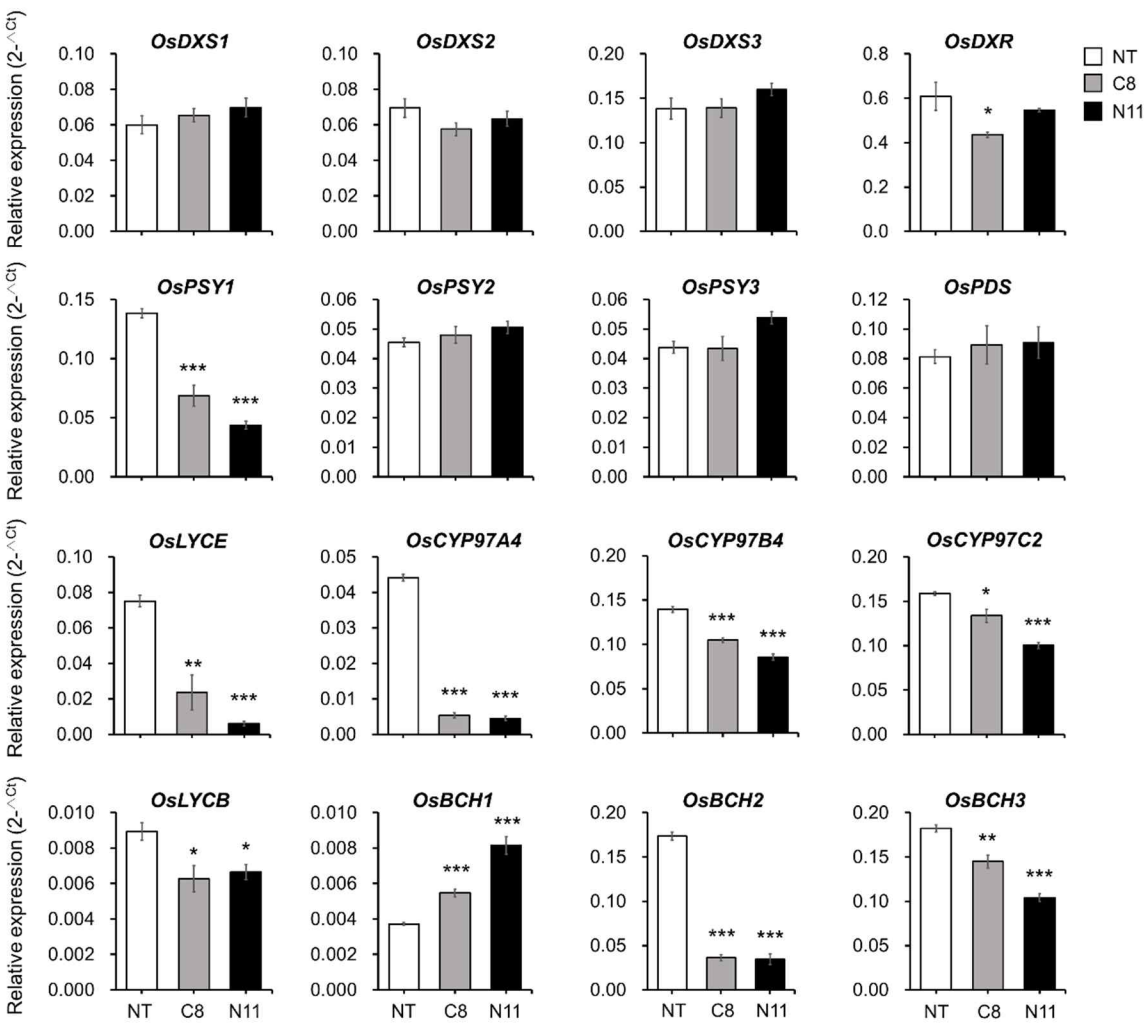
OsDXS1
OsDXS2
OsDXS3
OsDXR
OsPSY1
OsPSY2
OsPSY3
OsPDS
OsLYCE
OsCYP97A4
OsCYP97B4
OsCYP97C2
OsLYCB
OsBCH1
OsBCH2
OsBCH3
NT
C8
N11
Relative expression (2-^Ct)

F

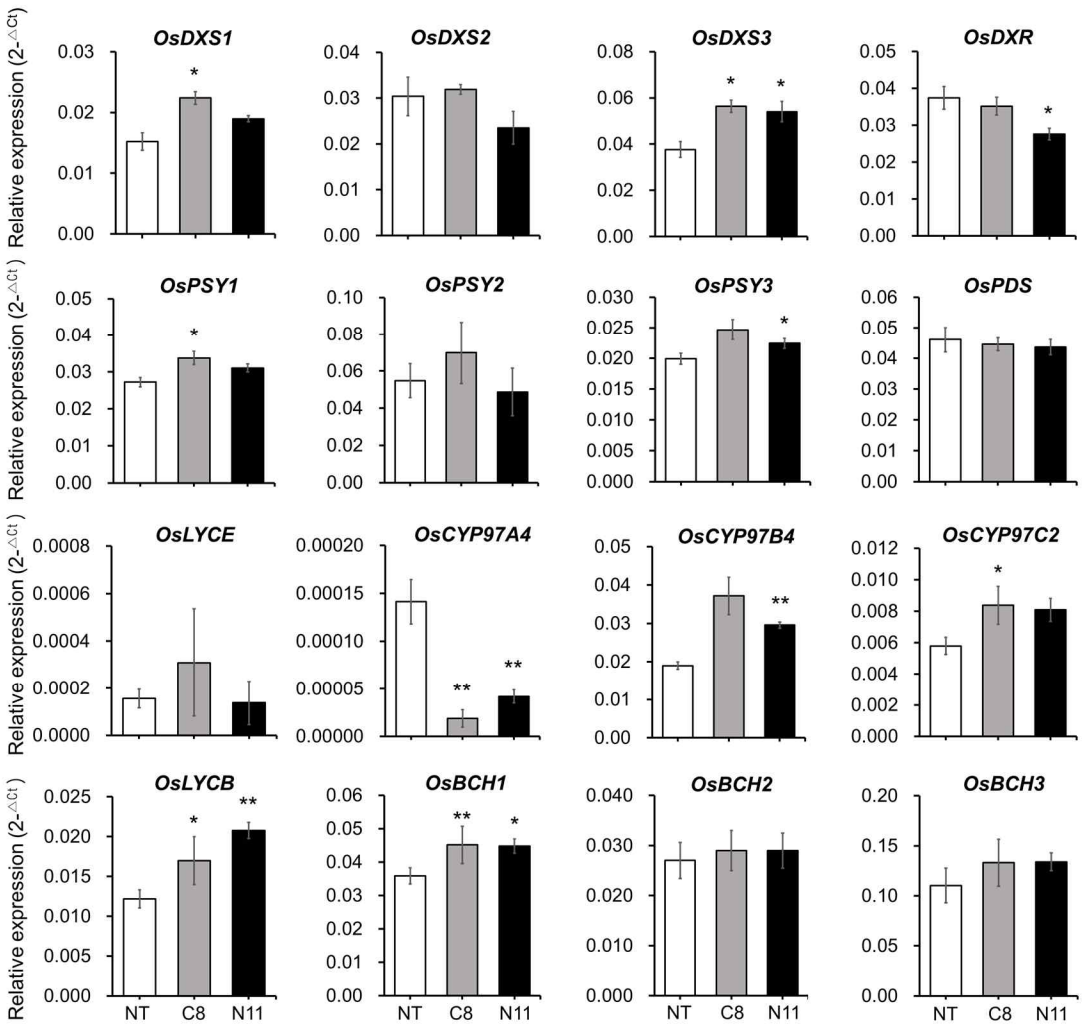
OsDXS1
OsDXS2
OsDXS3
OsDXR
OsPSY1
OsPSY2
OsPSY3
OsPDS
OsLYCE
OsCYP97A4
OsCYP97B4
OsCYP97C2
OsLYCB
OsBCH1
OsBCH2
OsBCH3
Relative expression (2-△Ct)
NT
C8
N11